1656 *Inorg. Chem.* **2011**, *50*, 1656–1669
DOI: 10.1021/ic102085b

Inorganic Chemistry
Article

Synthesis and Spectroscopic Characterization of CN-Substituted Bipyridyl Complexes of Ru(II)

Catherine E. McCusker and James K. McCusker*

Department of Chemistry, Michigan State University, East Lansing, Michigan 48824, United States

Received October 14, 2010

A series of ruthenium complexes having the general form $[Ru(bpy)_{3-n}(CN\text{-}Me\text{-}bpy)_n](PF_6)_2$ (where bpy = 2,2′-bipyridine, CN-Me-bpy = 4,4′-dicyano-5,5′-dimethyl-2,2′-bipyridine, and n = 1−3 for complexes **1**−**3**, respectively) have been synthesized and characterized using a variety of steady-state and nanosecond time-resolved spectroscopies. Electrochemical measurements indicate that the CN-Me-bpy ligand is significantly easier to reduce than the unsubstituted bipyridine (on the order of ∼500 mV), implying that the lowest energy ^{3}MLCT (metal-to-ligand charge transfer) state will be associated with the CN-Me-bpy ligand(s) in all three compounds. Comparison of the Huang−Rhys factors derived from spectral fitting analyses of the steady state emission spectra of complexes **1**−**3** suggests all three compounds are characterized by excited-state geometries that are less distorted relative to their ground states as compared to $[Ru(bpy)_3](PF_6)_2$; the effect of the more nested ground- and excited-state potentials is reflected in the unusually high radiative quantum yields (13% (**1**), 27% (**2**), and 40% (**3**)) and long ^{3}MLCT-state room-temperature lifetimes (1.6 μs, 2.6 μs, and 3.5 μs, respectively) for these compounds. Coupling of the π^* system into the CN groups is confirmed by nanosecond step-scan IR spectra which reveal a ∼40 cm^{-1} bathochromic shift of the CN stretching frequency, indicative of a weaker CN bond in the ^{3}MLCT excited state relative to the ground state. The fact that the shift is the same for complexes **1**−**3** is evidence that, in all three complexes, the long-lived excited state is localized on a single CN-Me-bpy ligand rather than being delocalized over multiple ligands.

Introduction

Photoinduced charge separation is the physical phenomenon underlying virtually all schemes geared toward the conversion of light into chemical, electrical, and/or mechanical energy.[1,2] Charge separation is typically effected in a molecular system through charge-transfer excited states, in which photon absorption causes charge redistribution within the chromophore: maintaining, amplifying, or, in the least favorable circumstances, destroying the resulting chemical potential depends on dynamics that occur within the chromophore immediately following the absorptive event.

Transition metal complexes having intense charge-transfer features have long been exploited to achieve the goal of creating reactive excited states for photochemical energy conversion.[3−10] Following excitation, a host of dynamic processes are potentially involved the subsequent relaxation of the initially formed excited state including intersystem crossing (ISC), internal conversion (IC), vibrational relaxation (VR), intramolecular vibrational redistribution (IVR), as well as solvation dynamics. In general, all of these fundamental processes can be categorized as either radiative or non-radiative in nature. With a few notable exceptions,[11−13] non-radiative dynamics—in particular vibrational relaxation—represent the dominant pathway(s) by which transition metal-based charge-transfer systems dissipate absorbed energy. Despite its central role in the photophysics of inorganic compounds—and in practical terms an important competing process for the efficient conversion of

*To whom correspondence should be addressed. E-mail: jkm@chemistry.msu.edu.

(1) Link, G.; Heinen, U.; Berthold, T.; Ohmes, E.; Weidner, J. U.; Kothe, G. *Z. Phys. Chem.* **2004**, *218*, 171–191.
(2) Santabarbara, S.; Galuppini, L.; Casazza, A. P. *J. Integr. Plant Biol.* **2010**, *52*, 735–749.
(3) Hagfeldt, A.; Grätzel, M. *Acc. Chem. Res.* **2000**, *33*, 269–277.
(4) Gratzel, M. *Inorg. Chem.* **2005**, *44*, 6841–6851.
(5) Hamann, T. W.; Jensen, R. A.; Martinson, A. B. F.; Ryswyk, H. V.; Hupp, J. T. *Energy Environ. Sci.* **2008**, *1*, 66–78.
(6) Grätzel, M. *Acc. Chem. Res.* **2009**, *42*, 1788–1798.
(7) Cao, Y.; Bai, Y.; Yu, Q.; Cheng, Y.; Liu, S.; Shi, D.; Gao, F.; Wang, P. *J. Phys. Chem. C* **2009**, *113*, 6290–6297.
(8) Bessho, T.; Zakeeruddin, S. M.; Yeh, C. Y.; Diau, E. W.; Grätzel, M. *Angew. Chem., Int. Ed.* **2010**, *49*, 6646–6649.
(9) Concepcion, J. J.; Jurss, J. W.; Brennaman, M. K.; Hoertz, P. G.; Patrocinio, A. O.; Murakami Iha, N. Y.; Templeton, J. L.; Meyer, T. J. *Acc. Chem. Res.* **2009**, *42*, 1954–1965.
(10) Magnuson, A.; Anderlund, M.; Johansson, O.; Lindblad, P.; Lomoth, R.; Polivka, T.; Ott, S.; Stensjo, K.; Styring, S.; Sundstrom, V.; Hammarstrom, L. *Acc. Chem. Res.* **2009**, *42*, 1899–1909.
(11) Flamigni, L.; Barbieri, A.; Sabatini, C.; Ventura, B. *Top. Curr. Chem.* **2007**, *281*, 143–203.
(12) Hofbeck, T.; Yersin, H. *Inorg. Chem.* **2010**, *49*, 9290–9299.
(13) Lamansky, S.; Djurovich, P.; Murphy, D.; Abdel-Razzaq, F.; Lee, H. E.; Adachi, C.; Burrows, P. E.; Forrest, S. R.; Thompson, M. E. *J. Am. Chem. Soc.* **2001**, *123*, 4304–4312.

 Published on Web 02/02/2011

light into more productive reaction pathways—relatively little is known concerning the mechanistic details by which vibrational relaxation occurs.

Probing vibrational relaxation in transition metal complexes is not straightforward. Information about this process can sometimes be inferred from transient electronic absorption spectroscopy.[14] As a molecule evolves from a vibrationally hot to a thermalized excited state, the associated dynamics can result in shifting and/or narrowing of an absorption feature over time. However, the precise details will depend greatly on the relative displacement and slope of the two excited state potential energy surfaces giving rise to the absorption. This makes it difficult to formulate useful generalizations for the interpretation of such observations. Time-resolved vibrational spectroscopy (i.e., infrared and/or Raman) is obviously a more direct way to probe vibrational dynamics in an electronic excited state. In general, formation of the Franck−Condon state will create a distribution of vibrationally excited states. These will ultimately relax to the ground vibrational level of the electronic excited state, causing the spectrum to narrow. In addition, the anharmonic nature of the potential surface means that the vibrational spacing is smaller near the top of the potential well than it is near the bottom: this will result in a blue shift in the absorption maximum. These experimental signatures have been used by a number of groups to directly monitor vibrational relaxation in electronic excited states.[15,16] Of particular relevance is the work of Browne, McGarvey, and co-workers, who employed time-resolved resonance Raman spectroscopy to monitor the formation of the thermalized ^{3}MLCT (metal-to-ligand charge transfer) state in $[Ru(bpy)_3]^{2+}$ by monitoring the growth of ring stretching and bending vibrations associated with the bipyridyl radical anion.[17,18] The success of this study notwithstanding, the presence of multiple overlapping bands in this region of the spectrum is nevertheless a complication that can mask more subtle changes in the peak shape and energy that accompany vibrational relaxation and/or IVR; interference from solvent vibrations is another potential problem in this regard. The situation becomes more problematic in the case of heteroleptic complexes, where even distinguishing among vibrations arising from different ligands can be difficult.[19]

As part of our research program to delineate the mechanism(s) of excited-state evolution in transition metal complexes, we sought to develop a system that would allow us to probe vibrational relaxation in charge-transfer excited states in a more straightforward fashion by incorporating an infrared tag into the chromophore. The ideal marker would be a functional group whose vibrations are spectrally isolated, is strongly coupled to the charge-transfer excited-state manifold of the system, and exhibits a significant and easily identifiable change in frequency between the ground and the excited state(s) of the system. Dynamics of metal carbonyl complexes have been examined using this principle; however, most of these compounds are not photostable (indeed, in these cases the CO stretch is used to monitor photodissociation reactions).[20−22] In cases where the CO group is not photochemically labile—$Re(bpy)(L)(CO)_3$ type systems, for example—the CO is an ancillary ligand and is therefore only indirectly coupled to the charge-transfer manifold.[23]

The cyano group is a less frequently used alternative to the carbonyl group but possesses many of the same desirable properties as CO. Its stretching frequency in the 2100−2300 cm^{-1} region of the spectrum is well removed from vibrations associated with the polypyridyl ligands typically employed in charge-transfer systems. It is sensitive to local environment—cyano-substituted amino acids have been used to probe secondary structure and environment in proteins[24]— allowing for the possiblilty to explore solvent effects. Terminal CN groups in metal dimer systems have proven useful for monitoring electron transfer reactions because of the shift in frequency upon oxidation/reduction of the bound metal center.[25−27] Finally, in work more directly relevant to our immediate goals, the potential utility of such a system has already been demonstrated by Vlček and co-workers who used the CN stretch of 4-cyano-pyridine to help assign the nature of the charge transfer transitions in $W(CO)_5$(4-CN-py).[15]

With these ideas in mind, herein we describe a series of complexes of the general form $[Ru(bpy)_{3-n}(CN\text{-}Me\text{-}bpy)_n](PF_6)_2$ (n = 1−3, where bpy is 2,2′-bipyridine and CN-Me-bpy is 4,4′-dicyano-5,5′-dimethyl-2,2′-bipyridine) which we are putting forward as a platform for the study of vibrational relaxation dynamics in a transition metal-based charge-transfer system. Incorporation of CN groups into the bipyridyl ligand introduces a vibrationally well-isolated infrared tag into the chromophore, while placement at the 4 and 4′ positions of the rings should lead to direct coupling of the CN group to the aromatic system of the bipyridine ring and make it extremely sensitive to electron density in the π^* orbital upon formation of the ligand radical anion in the MLCT excited state(s). As will become evident, the large difference in energy between the CN-Me-bpy and the unsubstituted ligand creates distinct MLCT absorption manifolds rather than one broadened one. This will allow selective placement of the Franck−Condon state on different parts of the chromophore and will facilitate, among other things, differentiation of IVR from vibrational cooling, as well as a comparison of conclusions drawn from direct measurement of vibrational

(14) Juban, E. A.; McCusker, J. K. *J. Am. Chem. Soc.* **2005**, *127*, 6857–6865.
(15) Záliš, S.; Busby, M.; Kotrba, T.; Matousek, P.; Towrie, M.; Vlček, A. A. *Inorg. Chem.* **2004**, *43*, 1723–1734.
(16) Maçôas, E. M.; Kananavicius, R.; Myllyperkiö, P.; Pettersson, M.; Kunttu, H. *J. Am. Chem. Soc.* **2007**, *129*, 8934–8935.
(17) Browne, W. R.; Coates, C. G.; Brady, C.; Matousek, P.; Towrie, M.; Botchway, S. W.; Parker, A. W.; Vos, J. G.; McGarvey, J. J. *J. Am. Chem. Soc.* **2003**, *125*, 1706–1707.
(18) Henry, W.; Coates, C. G.; Brady, C.; Ronayne, K. L.; Matousek, P.; Towrie, M.; Botchway, S. W.; Parker, A. W.; Vos, J. G.; Browne, W. R.; McGarvey, J. J. *J. Phys. Chem. A* **2008**, *112*, 4537–4544.
(19) Curtright, A. E.; McCusker, J. K. *J. Phys. Chem. A* **1999**, *103*, 7032–7041.
(20) Lian, T.; Bromberg, S. E.; Asplund, M. C.; Yang, H.; Harris, C. B. *J. Phys. Chem.* **1996**, *100*, 11994–12001.
(21) Farrell, I. R.; Matousek, P.; Vlček, A. A. *J. Am. Chem. Soc.* **1999**, *121*, 5296–5301.
(22) Portius, P.; Yang, J.; Sun, X.; Grills, D. C.; Matousek, P.; Parker, A. W.; Towrie, M.; George, M. W. *J. Am. Chem. Soc.* **2004**, *126*, 10713–10720.
(23) Liard, D. J.; Busby, M.; Matousek, P.; Towrie, M.; Vlček, A. A. *J. Phys. Chem. A* **2004**, *108*, 2363–2369.
(24) Lindquist, B. A.; Furse, K. E.; Corcelli, S. A. *Phys. Chem. Chem. Phys.* **2009**, *11*, 8119–8132.
(25) Doorn, S. K.; Dyer, R. B.; Stoutland, P. O.; Woodruff, W. H. *J. Am. Chem. Soc.* **1993**, *115*, 6398–6405.
(26) Wang, C.; Mohney, B. K.; Akhremitchev, B. B.; Walker, G. C. *J. Phys. Chem. A* **2000**, *104*, 4314–4320.
(27) Easun, T. L.; Alsindi, W. Z.; Deppermann, N.; Towrie, M.; Ronayne, K. L.; Sun, X. Z.; Ward, M. D.; George, M. W. *Inorg. Chem.* **2009**, *48*, 8759–8770.

dynamics versus those inferred from electronic absorption spectroscopy.[14,28]

As we have pointed out previously,[29] it is critical to have a detailed understanding of the properties of the ground and long-lived excited states of transition metal-based systems prior to the acquisition and interpretation of ultrafast data. This report therefore focuses on the synthesis, steady-state and nanosecond time-resolved spectroscopic characterization of the aforementioned series as a foundation for ultrafast spectroscopic studies of vibrational relaxation dynamics.

Experimental Section

General Procedures. All chemicals and solvents were obtained from Fisher or Aldrich Chemical Co. and used without further purification unless otherwise stated. $RuCl_3 \cdot xH_2O$, tris(benzylidineacetone)dipalladium(0) ($Pd_2(dba)_3$), and diphenylphosphinoferrocene (dppf) were purchased from Strem Chemicals, Inc., and C18 reversed phase silica gel was purchased from SiliCycle. NMR spectra were collected on Varian Inova-300 (300 MHz) or Varian UnityPlus-500 (500 MHz) spectrometers. Ground state infrared spectra (4000−400 cm^{-1}) were measured as KBr pellets using a Mattson Galaxy series 3000 FT-IR spectrophotometer. Mass spectra were obtained through the Michigan State University Mass Spectrometry Facility. Elemental analyses were obtained through the analytical facilities at Michigan State University or from Columbia Analytics.

4,4′-Dichloro-5,5′-dimethyl-2,2′-bipyridine (Cl-Me-bpy). a. 5,5′-Dimethyl-2,2′-bipyridine-*N*,*N*′-dioxide (5-dmb-*N*-oxide).[30] 5,5′-Dimethyl-2,2′-bipyridine (5.0 g) was dissolved in 35 mL of glacial acetic acid, and 7.0 mL of 30% hydrogen peroxide were slowly added. After heating the solution to 70−80 °C for 4 h, an additional 4.0 mL of 30% hydrogen peroxide were added, and the reaction mixture was heated overnight. The product was isolated by pouring the cooled solution over approximately 400 mL of acetone and reducing the volume under vacuum until a white precipitate formed. The white precipitate was collected by vacuum filtration, rinsed sparingly with acetone and ether, and then dried further under vacuum. Yield: 4.76 g (81%). ^{1}H NMR (300 MHz, D_2O): δ 8.19 (s, 2H′), 7.57 (d, J = 8.0 Hz, 2H), 7.14 (d, J = 8.0 Hz, 2H), 2.35 (s, 6H).

b. 5,5′-Dimethyl 4,4′-Dinitro-2,2′-bipyridine-*N*,*N*′-dioxide (NO_2-Me-bpy-*N*-oxide).[31,32] 5-dmb-*N*-oxide (4.5 g) was dissolved in 21 mL of sulfuric acid, and 9.0 mL of fuming nitric acid were slowly added to the solution. The solution was gently heated to 90−100 °C for 4 h. During the course of the reaction the mixture became yellow, and a brown gas formed above the solution. The solution was cooled to room temperature and slowly poured over ice formed by mixing 75 mL of water with excess liquid nitrogen. Additional liquid nitrogen was added, while stirring, to form a yellow slush. As the slush melted, a yellow precipitate was collected by vacuum filtration, rinsed thoroughly with water and ether, and then dried under vacuum. Yield: 3.75 g (59%). ^{1}H NMR (500 MHz, DMSO-d_6): δ 8.65 (s, 2H), 8.53 (s, 2H), 2.58 (s, 6H).

c. 4,4′-Dichloro-5,5′-Dimethyl-2,2′-bipyridine-*N*,*N*′-dioxide (Cl-Me-bpy-*N*-oxide).[33] NO_2-Me-bpy-*N*-oxide (3.75 g) was suspended in 55.0 mL of glacial acetic acid and 45.0 mL of acetyl chloride. The suspension was refluxed for 2 h, during which time the solution became clear yellow. The solution was cooled to room temperature and slowly poured over approximately 500 mL of ice. The resulting clear yellow solution was neutralized with concentrated sodium hydroxide, resulting in the formation of a white precipitate. The white solid was collected by vacuum filtration, rinsed with water and ether, and dried under vacuum. Yield: 3.13 g (90%). ^{1}H NMR (300 MHz, DMSO-d_6): δ 8.45 (s, 2H), 7.86 (s, 2H), 2.31 (s, 6H).

d. 4,4′-Dichloro-5,5′-dimethyl-2,2′-bipyridine (Cl-Me-bpy).[34] Cl-Me-bpy-*N*-oxide (3.13 g) was suspended in 460 mL of dry acetonitrile, and 21.0 mL of phosphorus trichloride were slowly added to the mixture. The suspension was refluxed under nitrogen for 4 h, after which the solution became a clear yellow color. The solution was cooled to room temperature and slowly poured over approximately 500 mL of ice. The solution was made basic (pH > 11) with the addition of concentrated sodium hydroxide resulting in the formation of a white precipitate. The white solid was collected by vacuum filtration, rinsed with water, and dried under vacuum. Concentrating the filtrate yielded additional product. Yield: 2.57 g (92%). ^{1}H NMR (500 MHz, $CDCl_3$): δ 8.47 (s, 2H), 8.37 (s, 2H), 2.42 (s, 6H). ^{13}C NMR (500 MHz, $CDCl_3$): δ 154.51, 150.85, 145.45, 132.44, 121.46, 16.94.

Bis(2,2′-bipyridine)(4,4′-dicyano-5,5′-dimethyl-2,2′-bipyridine)-ruthenium(II) Hexafluorophosphate ($[Ru(bpy)_2(CN\text{-}Me\text{-}bpy)](PF_6)_2$, (1)). a. Dichlorotetrakis(dimethyl sulfoxide)ruthenium-(II) $Ru(DMSO)_4Cl_2$. $Ru(DMSO)_4Cl_2$ was prepared by a modified version of the reported literature method.[35] Dimethyl sulfoxide (25.0 mL) was bubble degassed with nitrogen for 15 min, after which time 1.50 g of $RuCl_3 \cdot xH_2O$ were added to the solution. The reaction was gently heated under nitrogen for 30−45 min until the dark black-red solution became dark yellow-orange. The solution was cooled to room temperature, poured over 100 mL of acetone, and cooled in the freezer overnight to precipitate the product. The yellow microcrystalline solid was collected by vacuum filtration, rinsed once with acetone, rinsed three times with ether, and dried under vacuum. Yield: 2.20 g. Anal. Calcd (Found) for $C_8H_{24}Cl_2O_4S_4Ru \cdot 0.25(CH_3)_2SO$: C, 20.26 (20.14); H, 5.10 (5.23).

b. Bis(2,2′-bipyridine)dichlororuthenium(II) ($Ru(bpy)_2Cl_2$). $Ru(bpy)_2Cl_2$ was prepared from a modified version of the reported literature method, using $Ru(DMSO)_4Cl_2$ rather than $RuCl_3 \cdot xH_2O$.[36] Freshly distilled dimethylformamide (DMF, 35.0 mL) was bubble degassed with nitrogen for 15 min, and 1.60 g of $Ru(DMSO)_4Cl_2$, 1.10 g of 2,2′-bipyridine, and 7.30 g of LiCl were added to the solution. The solution was protected from light using aluminum foil and heated to reflux under nitrogen for approximately 4 h; the progress of the reaction was monitored using thin layer chromatography (silica, 10% acetone in dichloromethane). The dark purple reaction mixture was then cooled slightly after which the warm solution was poured over approximately 400 mL of acetone and cooled overnight in the freezer to precipitate the product. The dark precipitate was collected by vacuum filtration and rinsed with water to remove excess LiCl and a side product of $[Ru(bpy)_3]^{2+}$ until the filtrate was colorless. The remaining purple-green solid was rinsed three times with ether and dried under vacuum. Yield: 0.989 g (60%). Anal. Calcd (Found) for $C_{20}H_{16}Cl_2N_4Ru \cdot 1.0\ H_2O$: C, 47.82 (47.71); H, 3.61 (3.56); N, 11.15 (10.90). ^{1}H NMR (500 MHz, DMSO-d_6): δ 9.97 (d, J = 5.0 Hz, 2H), 8.65 (d, J = 8.1 Hz, 2H), 8.49 (d, J = 8.0 Hz, 2H), 8.07 (dt, J = 7.8, 1.26 Hz, 2H), 7.77 (dt, J = 6.6,1.0 Hz, 2H), 7.68 (dt, J = 7.8, 1.1 Hz, 2H), 7.52 (d, J = 5.6 Hz, 2H), 7.10 (dt J = 6.6, 1.1 Hz, 2H).

c. Bis(2,2′-bipyridine)(4,4′-dichloro-5,5′-dimethyl-2,2′-bipyridine)ruthenium(II) Hexafluorophosphate ($[Ru(bpy)_2(Cl\text{-}Me\text{-}bpy)](PF_6)_2$). Ethanol (30.0 mL) was bubble degassed with nitrogen for

(28) Damrauer, N. H.; McCusker, J. K. *J. Phys. Chem. A* **1999**, *103*, 8440–8446.
(29) McCusker, J. K. *Acc. Chem. Res.* **2003**, *36*, 876–887.
(30) Simpson, P. G.; Vinciguerra, A.; Quagliano, J. V. *Inorg. Chem.* **1963**, *2*, 282–286.
(31) Kavanagh, P.; Leech, D. *Tetrahedron Lett.* **2004**, *45*, 121–123.
(32) Mukkala, V. M.; Kankare, J. J. *Helv. Chim. Acta* **1992**, *75*, 1578–1592.
(33) Anderson, S.; Constable, E. C.; Seddon, K.; Turp, J. E.; Baggott, J. E.; Pilling, M. J. *J. Chem. Soc., Dalton Trans.* **1985**, 2247–2261.
(34) Wenkert, D.; Woodward, R. B. *J. Org. Chem.* **1983**, *48*, 283–289.
(35) Evans, I. P.; Spencer, A.; Wilkinson, G. *J. Chem. Soc., Dalton Trans.* **1973**, 204–209.
(36) Sullivan, B. P.; Salmon, D. J.; Meyer, T. J. *Inorg. Chem.* **1978**, *17*, 3334–3341.

15 min, and 0.59 g of $Ru(bpy)_2Cl_2$ and 0.33 g of Cl-Me-bpy were added to the solution. The solution was shielded from light and heated to reflux overnight under nitrogen. The solution was cooled to room temperature, and excess $NaPF_6$ dissolved in 50 mL of water was added to the solution to precipitate a red powder. The precipitate was collected by vacuum filtration, rinsed with water and ether, and dried under vacuum. The solid was recrystallized once by acetonitrile/ether diffusion. Yield: 0.849 g (73%). Anal. Calcd (Found) for $C_{32}H_{27}Cl_2F_{12}N_6P_2Ru \cdot 0.5\ H_2O$: C, 39.81 (39.60); H, 2.82 (2.80); N, 8.70 (8.63). ^{1}H NMR (500 MHz, CD_3CN): δ 8.51 (s, 2H), 8.48 (t, J = 8.5 Hz, 4H), 8.05 (m, J = 7.9 Hz, 4H), 7.75 (d, J = 5.6 Hz, 2H), 7.65 (d, J = 5.6 Hz, 2H), 7.51 (s, 2H), 7.41 (dt, J = 6.6, 1.3 Hz, 2H), 7.37 (dt J = 6.7, 1.3 Hz, 2H), 2.20 (s, 6H). ^{13}C NMR (500 MHz, CD_3CN): δ 158.38, 158.33, 156.32, 153.86, 153.18, 152.98, 146.90, 139.19, 139.17, 138.52, 128.96, 128.77, 125.78, 125.65, 125.64, 17.71. MS [ESI (CH_3CN), m/z (rel. int.)]: 333.1 (100) $[M - 2PF_6]^{2+}$, 811.2 (68) $[M - PF_6]^{1+}$.

d. Bis(2,2′-bipyridine)(4,4′-dicyano-5,5′-dimethyl-2,2′-bipyridine)ruthenium(II) Hexafluorophosphate ([Ru(bpy)$_2$(CN-Me-bpy)](PF$_6$)$_2$, (1)). This synthesis is a modified version of the reported synthesis for 4′-cyano-2,2′:6′,2″-terpyridine complexes of ruthenium.[37] Anhydrous dimethylacetamide (DMA) was degassed using freeze−pump−thaw techniques prior to use. $[Ru(bpy)_2(Cl\text{-}Me\text{-}bpy)](PF_6)_2$ (0.500 g), zinc cyanide (0.740 g), $Pd_2(dba)_3$ (0.045 g), dppf (0.060 g), zinc dust (0.200 g), and DMA (80.0 mL) were combined in an inert atmosphere glovebox. The solution was transferred from the glovebox to a Schlenk line, shielded from light, and heated slowly under nitrogen. The progress of the reaction was monitored by electronic absorption spectroscopy. After the reaction was complete (i.e., when no further changes in the absorption spectrum were noted, ca. 1 h), the solution was cooled to room temperature and filtered through Celite. The filtrate was evaporated to near dryness under vacuum, and the dark red-orange residue was dissolved in acetonitrile and precipitated with ether. The resulting orange solid was collected by vacuum filtration and washed with ether. The solid was recrystallized once by acetonitrile/ether diffusion and then purified twice by column chromatography using neutral alumina and C-18 reverse phase silica gel with 7:1 acetonitrile/aqueous KNO_3 as the eluent for both columns. After the column purification the product was recrystallized by acetonitrile/ether diffusion to remove excess nitrate salts from the column eluent. Yield: 0.309 g (63%). Anal. Calcd (Found) for $C_{34}H_{26}F_{12}N_8P_2Ru$: C, 43.55(43.40); H, 2.79 (2.85); N, 11.95 (11.84); Ru, 10.78 (10.11). ^{1}H NMR (500 MHz, CD_3CN): δ 8.69 (s, 2H), 8.49 (t, J = 7.8 Hz, 4H), 8.08 (m, J = 7.9, 1.5 Hz, 4H), 7.78 (s, 2H), 7.64 (dd, J = 12.6, 5.5 Hz, 4H), 7.41 (m, J = 7.08, 1.3 Hz, 4H), 2.38 (s, 6H). ^{13}C NMR (500 MHz, CD_3CN): δ 156.88, 156.56, 154.54, 153.52, 151.95, 151.54, 140.52, 138.49, 138.41, 127.90, 127.60, 126.21, 124.57, 124.54, 121.22, 114.80, 17.12. MS [ESI (CH_3CN), m/z (rel. int.)]: 324.0 (95) $[M - 2PF_6]^{2+}$, 793.1 (100) $[M - PF_6]^{1+}$. MS [HR-ESI (CH_3CN)] m/z 793.0973 $[M - PF_6]^{1+}$, calcd ($C_{34}H_{26}N_8F_6PRu$) 793.0966. FT-IR (selected frequencies in KBr pellet, cm^{-1}) 3117(w), 2234(m), 1605(m), 1467(s), 1447(s), 1241(m), 839(vs), 762(s), 557(vs). Electronic absorption (CH_3CN) λ, nm (ε, M^{-1} cm^{-1}): 285 (63,800) 318 (36,700), 420 (13,400) 479 (14,000).

(2,2′-Bipyridine)bis(4,4′-dicyano-5,5′-dimethyl-2,2′-bipyridine)ruthenium(II) Hexafluorophosphate ([Ru(bpy)(CN-Me-bpy)$_2$](PF$_6$)$_2$, (2)). This molecule was synthesized in the same manner as $[Ru(bpy)_2(CN\text{-}Me\text{-}bpy)](PF_6)_2$, starting from the appropriate Cl-Me-bpy ruthenium complex.

a. Bis(4,4′-dichloro-5,5′-dimethyl-2,2′-bipyridine)dichlororuthenium(II) (Ru(Cl-Me-bpy)$_2$Cl$_2$). Freshly distilled DMF (20.0 mL) was bubble degassed for 15 min, and 0.810 g of $Ru(DMSO)_4Cl_2$, 0.850 g of Cl-Me-bpy, and 8.00 g of LiCl were added to the solution. The solution was protected from light with aluminum foil and heated to reflux under nitrogen for 2 h. The dark purple reaction mixture was then cooled slightly after which the warm solution was poured over approximately 400 mL of acetone and cooled overnight in the freezer to precipitate the product. The dark precipitate was collected by vacuum filtration and rinsed with water to remove excess LiCl and a side product of $[Ru(Cl\text{-}Me\text{-}bpy)_3]^{2+}$ until the filtrate was colorless. The remaining dark purple solid was rinsed with ether and dried under vacuum. The product was recrystallized once by dichloromethane/ether diffusion. Yield: 0.747 g (66%). ^{1}H NMR (500 MHz, DMSO-d_6): δ 9.72 (s, 2H), 8.89 (s, 2H), 8.75 (s, 2H), 7.53 (s, 2H), 2.53 (s, 6H), 2.10 (s, 6H).

b. (2,2′-Bipyridine)bis(4,4′-dichloro-5,5′-dimethyl-2,2′-bipyridine)ruthenium(II) Hexafluorophosphate ([Ru(bpy)(Cl-Me-bpy)$_2$](PF$_6$)$_2$). A 30.0 mL volume of ethanol was bubble degassed with nitrogen for 15 min, and 0.500 g of $Ru(Cl\text{-}Me\text{-}bpy)_2Cl_2$ and 0.120 g of 2,2′-bipyridine were added. The reaction was shielded from light and heated to reflux, under nitrogen, overnight. The solution was cooled to room temperature, and excess $NaPF_6$ dissolved in 50.0 mL of water was added to precipitate a red powder. The precipitate was collected by vacuum filtration, rinsed with water and ether, and dried under vacuum. The red powder was recrystallized once by acetonitrile/ether diffusion. Yield: 0.681 g (88%). Anal. Calcd (Found) for $C_{34}H_{28}Cl_4F_{12}N_6P_2Ru \cdot 0.5\ H_2O$: C, 38.43 (38.74); H, 2.75 (2.87); N, 7.91 (8.13). ^{1}H NMR (500 MHz, CD_3CN): δ 8.51 (s, 2H), 8.49 (s, 2H), 8.47 (d, J = 7.9 Hz 2H), 8.06 (dt, J = 7.9, 1.3 Hz, 2H), 7.70 (d, J = 5.7 Hz, 2H), 7.55 (s, 2H), 7.41 (s, 2H), 7.39 (dt, J = 6.6, 1.3 Hz, 2H), 2.25 (s, 6H), 2.18 (s, 6H). ^{13}C NMR (500 MHz, CD_3CN): δ 158.43, 156.42, 156.40, 154.03, 153.84, 153.23, 147.07, 147.04, 139.34, 138.59, 138.56, 128.91, 125.89, 125.80, 17.84, 17.67. MS: [ESI, m/z (rel. int.)]: 382.1 (100) $[M - 2PF_6]^{2+}$, 909.1 (67) $[M - PF_6]^{1+}$.

c. (2,2′-Bipyridine)bis(4,4′-dicyano-5,5′-dimethyl-2,2′-bipyridine)ruthenium(II) Hexafluorophosphate ([Ru(bpy)(CN-Me-bpy)$_2$](PF$_6$)$_2$, (2)). $[Ru(bpy)(CN\text{-}Me\text{-}bpy)_2](PF_6)_2$ was synthesized in the same manner as $[Ru(bpy)_2(CN\text{-}Me\text{-}bpy)](PF_6)_2$ using 0.300 g of $[Ru(bpy)(Cl\text{-}Me\text{-}bpy)_2](PF_6)_2$, 0.400 g of zinc cyanide, 0.051 g of $Pd_2(dba)_3$, 0.063 g of dppf, 0.300 g of zinc dust, and 60.0 mL of DMA. Yield: 0.116 g (40%). Anal. Calcd (Found) for $C_{38}H_{28}F_{12}N_{10}P_2Ru \cdot 1.5\ H_2O$: C, 43.77 (43.89); H, 2.99 (2.72); N, 13.43 (13.20); Ru, 9.69 (8.94). ^{1}H NMR (500 MHz, CD_3CN): δ 8.70 (s, 2H), 8.68(s, 2H), 8.50 (d, J = 7.9 Hz, 2H), 8.12 (dt, J = 7.9 Hz, 1.5, 2H), 7.68 (t, J = 0.7 Hz, 2H), 7.64 (t, J = 0.7 Hz, 2H) 7.58 (d, J = 5.3 Hz, 2H), 7.42 (dt, J = 6.7, 1.3 Hz, 2H), 2.41 (s, 6H), 2.37 (s, 6H). ^{13}C NMR (500 MHz, CD_3CN): δ 157.90, 155.74, 155.45, 155.10, 154.80, 153.21, 142.25, 142.15, 140.34, 129.26, 127.77, 127.76, 126.22, 123.36, 123.27, 116.04, 116.02, 18.65, 18.44. MS [ESI (CH_3CN), m/z (rel. int.)]: 363.1 (100) $[M - 2PF_6]^{2+}$, 871.1 (48) $[M - PF_6]^{1+}$. MS [HR-ESI (CH_3CN)] m/z 871.1166 $[M - PF_6]^{1+}$, calcd ($C_{38}H_{28}N_{10}F_6PRu$) 871.1184. FT-IR (selected frequencies in KBr pellet, cm^{-1}) 3117(w), 2920(w), 2236(s), 1607(m), 1478(s), 1384(s), 1241(m), 841(vs), 765(m), 562(vs). Electronic absorption (CH_3CN) λ, nm (ε, M^{-1} cm^{-1}): 284 (37,000), 317 (55,200), 367 (12,800), 440 (12,600), 477 (16,700).

Tris(4,4′-dicyano-5,5′-dimethyl-2,2′-bipyridine)ruthenium(II) Hexafluorophosphate ([Ru(CN-Me-bpy)$_3$](PF$_6$)$_2$, (3)). This molecule was synthesized in the same manner as $[Ru(bpy)_2(CN\text{-}Me\text{-}bpy)](PF_6)_2$, starting from the appropriate Cl-Me-bpy ruthenium complex.

a. Tris(4,4′-dichloro-5,5′-dimethyl-2,2′-bipyridine)ruthenium(II) Hexafluorophosphate ([Ru(Cl-Me-bpy)$_3$](PF$_6$)$_2$). Ethanol (30 mL) was bubble degassed with nitrogen for 15 min, and 0.260 g of $Ru(DMSO)_4Cl_2$ and 0.530 g of Cl-Me-bpy were added to the solution. The reaction was shielded from light and heated to reflux for 48 h under nitrogen. The solution was cooled to room temperature, and excess $NaPF_6$, dissolved in 50.0 mL of water,

(37) Wang, J.; Fang, Y.; Hanan, G. S.; Loiseau, F.; Campagna, S. *Inorg. Chem.* **2005**, *44*, 5–7.

was added to precipitate a red powder. The precipitate was collected by vacuum filtration, rinsed well with water and ether, and dried under vacuum. The solid was recrystallized once by acetonitrile/ether diffusion. Yield: 0.385 g (63%). Anal. Calcd (Found) for $C_{36}H_{30}Cl_6F_{12}N_6P_2Ru$: C, 37.59 (37.17); H, 2.63 (2.62); N, 7.31 (7.25). ^{1}H NMR (500 MHz, CD_3CN): δ 8.49 (s, 2H), 7.48 (s, 2H), 2.23 (s, 6H). ^{13}C NMR (500 MHz, CD_3CN): δ 156.33, 153.88, 147.11, 138.57, 125.91, 17.68. MS [ESI, m/z (rel. int.)]: 430.1 (100) $[M - 2PF_6]^{2+}$, 1005.1 (55) $[M - PF_6]^{1+}$.

b. Tris(4,4′-dicyano-5,5′-dimethyl-2,2′-bipyridine)ruthenium(II) Hexafluorophosphate ($[Ru(CN\text{-}Me\text{-}bpy)_3](PF_6)_2$, (3)). $[Ru(CN\text{-}Me\text{-}bpy)_3](PF_6)_2$ was synthesized in the same manner as $[Ru(bpy)_2(CN\text{-}Me\text{-}bpy)](PF_6)_2$ using 0.630 g of $[Ru(Cl\text{-}Me\text{-}bpy)_3](PF_6)_2$, 1.90 g of zinc cyanide, 0.160 g of $Pd_2(dba)_3$, 0.180 g of dppf, 0.500 g of zinc dust, and 125 mL of DMA. Yield: 0.117 g (20%). Anal. Calcd (Found) for $C_{42}H_{30}F_{12}N_{12}P_2Ru \cdot 1.75\ CH_3CN$: C, 46.89 (47.29); H, 3.05 (2.77); N, 16.52 (16.11); Ru, 8.67 (8.29). ^{1}H NMR (500 MHz, CD_3CN): δ 8.71 (s, 2H), 7.59 (s, 2H), 2.41 (s, 6H). ^{13}C NMR (500 MHz, CD_3CN): δ 155.33, 154.99, 142.50, 128.01, 123.83, 115.95, 18.51. MS [ESI (CH_3CN), m/z (rel. int.)]: 402.1(100) $[M - 2PF_6]^{2+}$, 949.1 (10) $[M - PF_6]^{1+}$. MS [HR-ESI (CH_3CN)] m/z 949.1413 $[M - PF_6]^{1+}$, calcd ($C_{42}H_{30}N_{12}F_6PRu$) 949.1402. FT-IR (selected frequencies in KBr pellet, cm^{-1}) 3050(w), 2235(m), 1631(m), 1477(s), 1385(s), 1242(m), 842(vs), 558(vs). Electronic absorption (CH_3CN) λ, nm (ε, $M^{-1}\ cm^{-1}$): 315 (78,800), 458 (23,000).

Physical Measurements

Electrochemistry and Spectroelectrochemistry. Electrochemical measurements were carried out in an Ar-filled glovebox (Vacuum Atmospheres) using a CHI 630B electrochemical analyzer. A standard three-electrode arrangement was used consisting of a Pt working electrode, a graphite counter electrode, and a Ag/AgCl reference electrode (Cypress Systems). Measurements were carried out in spectrophotometric grade CH_3CN, which was freeze−pump−thaw degassed before use, and using 0.1 M tetrabutylammonium hexafluorophosphate ($TBAPF_6$) as the supporting electrolyte. Data were acquired by cyclic voltammetry (CV) and differential pulse voltammetry (DPV); the scan rate for the CV measurements was 50 mV/s and the scan rate and pulse width for the DPV measurements were 20 mV/s and 50 mV, respectively. Values for $E_{1/2}$ obtained by the two techniques were comparable. All oxidation and reduction waves were reversible over several successive scans. Potentials are listed versus the ferrocene/ferrocenium couple, which was used as an internal standard, and quoted as $E_{1/2}$ values as calculated from the DPV peak potentials.[38]

UV−visible spectroelectrochemical experiments were performed in a 1 mm path length spectroelectrochemical cell (CH Instruments) with a Ag/AgCl reference electrode inside an Ar filled glovebox. Measurements were carried out in spectrophotometric grade CH_3CN, which was freeze−pump−thaw degassed before use, and using 0.1 M $TBAPF_6$ as the supporting electrolyte. Samples were dissolved in the electrolyte solution to give an absorbance of 0.3−0.5 at the maximum of the main absorption band in the visible region. Difference spectra were collected on a SI440 CCD spectrometer in ca. 30 s intervals as the samples were oxidized or reduced. Oxidative spectra were collected at a potential 100 mV more positive than $E_{1/2}^{ox}$; reductive spectra were collected at a potential 100 mV more negative than $E_{1/2}^{red1}$ or halfway between $E_{1/2}^{red1}$ and $E_{1/2}^{red2}$, whichever was less reducing.

Electronic Steady-State and Time-Resolved Spectroscopies. All spectra were collected in spectrophotometric grade CH_3CN unless otherwise noted. For steady-state and time-resolved measurements, the solvent was freeze−pump−thaw degassed before use. Electronic absorption spectra for all compounds were acquired using a Cary 50 spectrophotometer. Steady-state emission spectra were acquired following MLCT excitation using a Spex Fluoromax fluorimeter and corrected for instrumental response using a NIST standard of spectral irradiance (Optronic Laboratories, Inc., OL220 M tungsten quartz lamp). Samples were prepared in an inert atmosphere glovebox in 1 cm quartz cuvettes and measured under optically dilute conditions (o. d. 0.1−0.2). The resulting emission spectra were fit with an asymmetric double sigmoidal function using IGOR pro. This function has no mathematical significance but is able to accurately reproduce the shape of the entire emission curve and thereby capture the small area (<10%) that lies outside of the detector range. This results in a more accurate estimate of the integrated spectrum. Relative radiative quantum yields (Φ_r) were determined using $[Ru(bpy)_3](PF_6)_2$ as a standard ($\Phi_{std} = 0.095$ in degassed CH_3CN[39]). Quantum yields were calculated using eq 1,

$$\phi_{unk} = \phi_{std} \cdot \left(\frac{I_{unk}/A_{unk}}{I_{std}/A_{std}}\right) \cdot \left(\frac{\eta_{unk}}{\eta_{std}}\right)^2 \quad (1)$$

where Φ_{unk} is the relative radiative quantum yield of the sample, I_{unk} and I_{std} are the integrated areas of the corrected emission spectra of the sample and standard respectively, A_{unk} and A_{std} are the absorbances of the sample and the standard at the excitation wavelength, and η_{unk} and η_{std} are the indexes of refraction of the respective solvents (taken to be equal to the neat solvents in both cases). Low-temperature emission spectra were collected using a Janis SVT-100 optical cryostat as described previously.[40] Measurements were taken at 80 K in a 9:2 mixture of butyronitrile and propionitrile, both of which were freeze−pump−thaw degassed before use. Estimates of the zero point energy gap (E_0), Huang−Rhys factor (S_M), energy of the average vibrational mode coupling the ground and excited states ($\bar{h}\omega_M$), and spectral bandwidth ($\Delta\bar{\nu}_{0,1/2}$) were determined by a single mode fit of the steady-state emission spectra to eq 2 as described by Claude and Meyer.[41]

$$I(\bar{\nu}) = \sum_{\nu_M=0}^{5} \left\{ \left(\frac{E_0 - \nu_M \hbar\omega_M}{E_0}\right)^3 \cdot \frac{S_M^{\nu_M}}{\nu_M!} \cdot \exp\left(-4(\ln 2)\left(\frac{\bar{\nu} - E_0 + \nu_M \hbar\omega_M}{\Delta\bar{\nu}_{0,1/2}}\right)^2 \right) \right\} \quad (2)$$

The correction of Parker and Rees was applied to all spectra when converting from wavelength to energy units.[42]

(38) Richardson, D. E.; Taube, H. *Inorg. Chem.* **1981**, *20*, 1278–1285.

(39) Suzuki, K.; Kobayashi, A.; Kaneko, S.; Takehira, K.; Yoshihara, T.; Ishida, H.; Shiina, Y.; Oishi, S.; Tobita, S. *Phys. Chem. Chem. Phys.* **2009**, *11*, 9850–9860.

(40) Damrauer, N. H.; McCusker, J. K. *Inorg. Chem.* **1999**, *38*, 4268–4277.

(41) Claude, J. P.; Meyer, T. J. *J. Phys. Chem.* **1995**, *99*, 51–54.

(42) Parker, C. A.; Rees, W. T. *Analyst* (*London*) **1960**, *85*, 587–600.

Nanosecond time-resolved emission and transient absorption experiments were carried out using a Nd:YAG laser spectrometer that has been described previously.[43,44] Time-resolved emission data were collected on the same samples used to acquire the room-temperature steady-state emission spectra (vide supra). Samples for time-resolved absorption measurements were prepared with an absorbance in the range of 0.3−0.5 at the excitation wavelength (500 nm for **1** and **2** and 480 nm for **3**) and sealed under an Ar atmosphere in 1 cm pathlength quartz cuvettes. The reported data correspond to 15 shot averages of the signal and baseline as well as background sample emission, all acquired at 0.2 Hz, with 1−3 mJ of pump power at the sample. The baseline and emission were subsequently subtracted from the signal and the data analyzed using a program of local origin. All data were checked for linearity with respect to pump power. In addition, absorption spectra were measured before and after all time-resolved absorption experiments to ensure the integrity of the sample. For full spectrum data acquisition, the laser power was periodically monitored to ensure constant pulse energy over the course of the experiment. Data acquired at each probe wavelength were fit to a single exponential kinetic model; the amplitudes for each of these fits were plotted to produce the differential absorption spectra reported herein.

Nanosecond Time-Resolved Infrared Spectroscopy. Nanosecond time-resolved step-scan infrared (SSIR) absorption spectra were measured on a step-scan modified Bruker IFS66 FTIR spectrometer with a standard globar source and nitrogen purge. Nitromethane was used as the solvent in these experiments; emission measurements on complex **1** in CH_3CN and CH_3NO_2 showed no significant differences in the emission profile or lifetime. The compounds were dissolved in dried CH_3NO_2 to give a ground state infrared absorption of 0.2−0.6 for the $\tilde{\nu}$(CN) band (10−20 mM). All solutions were deoxygenated by bubbling with nitrogen for 15 min. Spectra were measured in a demountable CaF_2 cell with a 0.5 mm or 1 mm Teflon spacer (Specac). Samples were excited using an OPOTEK Vibrant Nd:YAG laser (∼3−4 mJ/pulse, 10 Hz). Excitation wavelengths within the lowest energy visible absorption feature were chosen such that the absorbance was less than 2 to ensure uniform excitation of the sample. An AC/DC-coupled photovoltaic Kolmar Technologies mercury cadmium telluride (PV MCT) detector with a 20 MHz preamplifier was used to sample the transmitted IR probe beam. The detector's AC signal was further amplified (25×) with a 350 MHz fast preamplifier (Stanford Research SR445A) before being directed to a 100/200 MHz PAD82a transient digitizer board. The interferogram response before and after laser excitation was collected in 10 ns time slices, with 30 laser shots averaged at each mirror position. For each scan, folding limits of 2600 and 1000 cm^{-1} at 4 cm^{-1} resolution resulted in 1332 mirror positions. The DC signal was collected separately and used to check for sample decomposition as well as for phase correction of the AC signal. Bruker Instruments' Opus 5.5 software was used to process the recorded data. Differential absorbance spectra were calculated from the AC and DC single channel spectra as described previously.[45] The differential excited state absorption spectra reported herein represent an average of 4−8 scans, ground state spectra correspond to an average of 30 (rapid) scans.

Calculations. Calculations on complex **1** were performed using the Gaussian 03 software package.[46] Geometry optimizations were done on both the ground state and the lowest energy triplet charge-transfer excited state using a spin unrestricted formalism at the B3LYP/LANL2DZ level of theory.[47,48] No symmetry restrictions were placed on the geometry optimizations. The effect of the acetonitrile solvent environment was included by using the polarizable continuum model (PCM). Frequency calculations were performed on both the singlet and the triplet optimized structures to ensure that these geometries corresponded to global minima: no imaginary frequencies were obtained for either of the optimized geometries. Orbitals derived from these calculations were visualized using GaussView.

Results and Discussion

We have prepared a series of cyano-substituted ruthenium polypyridyl complexes with the general form $[Ru(bpy)_{3-n}(CN\text{-}Me\text{-}bpy)_n](PF_6)_2$. These complexes have been designed to combine the well documented charge transfer properties of the ruthenium polypyridyl complexes with a cyanide infrared tag to enable the study of vibrational relaxation dynamics in charge transfer excited states. This report describes the synthesis and spectroscopic characterization of this series, thus providing the necessary foundation for a detailed study of vibrational relaxation dynamics in a prototypical MLCT chromophore.

Synthesis. The synthesis of ruthenium complexes is well established, versatile, and can be carried out using bipyridine ligands having electron-withdrawing substituents such as such as nitro, trifluoromethyl, and ethyl ester.[49−53] However, initial attempts to synthesize ruthenium complexes of 4,4′-dicyano-2,2′-bipyridine (CN-bpy) using a variety of reaction conditions led to only trace amounts of the desired products even with extended (i.e., weeks to months) reaction time. The fact that examples of ruthenium

(43) Damrauer, N. H.; Boussie, T. R.; Devenney, M.; McCusker, J. K. *J. Chem. Soc.* **1997**, *119*, 8253–8268.
(44) Picraux, L. B.; Smeigh, A. L.; Guo, D.; McCusker, J. K. *Inorg. Chem.* **2005**, *44*, 7846–7865.
(45) Sun, H.; Frei, H. *J. Phys. Chem. B* **1997**, *101*, 205–209.
(46) Frisch, M. J.; Trucks, G. W.; Schlegel, H. B.; Scuseria, G. E.; Robb, M. A.; Cheeseman, J. R.; Montgomery, J., J. A.; Vreven, T.; Kudin, K. N.; Burant, J. C.; Millam, J. M.; Iyengar, S. S.; Tomasi, J.; Barone, V.; Mennucci, B.; Cossi, M.; Scalmani, G.; Rega, N.; Petersson, G. A.; Nakatsuji, H.; Hada, M.; Ehara, M.; Toyota, K.; Fukuda, R.; Hasegawa, J.; Ishida, M.; Nakajima, T.; Honda, Y.; Kitao, O.; Nakai, H.; Klene, M.; Li, X.; Knox, J. E.; Hratchian, H. P.; Cross, J. B.; Bakken, V.; Adamo, C.; Jaramillo, J.; Gomperts, R.; Stratmann, R. E.; Yazyev, O.; Austin, A. J.; Cammi, R.; Pomelli, C.; Ochterski, J. W.; Ayala, P. Y.; Morokuma, K.; Voth, G. A.; Salvador, P.; Dannenberg, J. J.; Zakrzewski, V. G.; Dapprich, S.; Daniels, A. D.; Strain, M. C.; Farkas, O.; Malick, D. K.; Rabuck, A. D.; Raghavachari, K.; Foresman, J. B.; Ortiz, J. V.; Cui, Q.; Baboul, A. G.; Clifford, S.; Cioslowski, J.; Stefanov, B. B.; Liu, G.; Liashenko, A.; Piskorz, P.; Komaromi, I.; Martin, R. L.; Fox, D. J.; Keith, T.; Al-Laham, M. A.; Peng, C. Y.; Nanayakkara, A.; Challacombe, M.; Gill, P. M. W.; Johnson, B.; Chen, W.; Wong, M. W.; Gonzalez, C.; Pople, J. A. *Gaussian 03*, revision D.01; Gaussian, Inc.: Wallingford, CT, 2004.
(47) Monat, J. E.; Rodriguez, J. H.; McCusker, J. K. *J. Phys. Chem. A* **2002**, *106*, 7399–7406.
(48) Fodor, L.; Lendvay, G.; Horváth, A. *J. Phys. Chem. A* **2007**, *111*, 12891–12900.
(49) Cook, M. J.; Lewis, A. P.; McAuliffe, G. S. G.; Skarda, V.; Thomson, A. J.; Glasper, J. L.; Robbins, D. J. *J. Chem. Soc., Perkin Trans.* **1984**, *417*, 1293–1301.

complexes containing cyano-substituted bipyridine ligands have been reported in the literature suggests that $[Ru(bpy)_{3-n}(CN\text{-}bpy)_n]^{2+}$ ($n = 1-3$) complexes are thermodynamically stable, implying that kinetic factors are likely responsible for the low yields of the CN-bpy complexes by these routes.[54,55]

One alternate pathway to form ruthenium complexes of CN-bpy is to carry out the cyanide functionalization after the ligand is bound to the metal center. There are many examples of such transformations in the literature, circumventing difficult purifications, insoluble intermediates, and/or kinetically unfavorable reactions.[56−61] In particular, palladium catalysts have proven effective in converting aryl halides to cyanides in high yields;[62,63] Hanan, Campagna, and co-workers have demonstrated that this reaction can also be used on ruthenium complexes.[37] Starting from the chloro-substituted ruthenium bipyridine complexes, we were able to synthesize ruthenium complexes of 4,4′-dicyano-2,2′-bipyridine, proving that the desired complexes are indeed thermodynamically viable. Unfortunately, these complexes were highly susceptible to hydrolysis to form the corresponding amide, especially during column chromatography as well as subsequent to reduction during electrochemical measurements. To increase the basicity of the nitrogens and (hopefully) increase the stability of the complexes, electron donating methyl groups were added to the 5 and 5′ positions of the bipyridine ring. This approach proved to be successful, yielding the final $[Ru(bpy)_{3-n}(CN\text{-}Me\text{-}bpy)_n]^{2+}$ ($n = 1-3$) complexes, shown in Scheme 1, which could withstand column chromatography as well as exhibiting reversible electrochemistry.

The synthesis of the desired complexes took place in three stages. First, the Cl-Me-bpy ligand was synthesized via the nitro-substituted intermediate using the literature procedure reported for 4,4-dichloro-2,2′-bipyridine.[30−34] The ruthenium complexes of the Cl-Me-bpy ligand were then synthesized using well-established literature methods. For the final step of synthesizing the CN-Me-bpy ruthenium complexes, the procedure Hanan, Campagna, and coworkers reported for $[Ru(tpy)(CN\text{-}tpy)]^{2+}$ and $[Ru(CN\text{-}tpy)_2]^{2+}$(CN-tpy = 4′-cyano-2,2′:6′,2″-terpyridine) had to be modified for these bipyridine-based reactions. The amount of palladium catalyst and ligand were kept the same as reported (5 and 10 mol % per CN group respectively); however, we found that an excess of zinc cyanide (as opposed to the stoichiometric amount used for the tpy-based systems) was necessary to form the bipyridine complexes. In addition, the 6−12 h reaction time necessary for the terpyridine complexes had to be truncated to 1−2 h for the bipyridine analogues to avoid the formation of side products that were not easily removed by recrystallization or column chromatography. The ideal reaction time differed depending on the exact rate of heating (~1 °C/minute was used), so monitoring the reaction progress by electronic absorption spectroscopy (Supporting Information, Figures S1−S3) was essential for determining when the reaction had reached completion. Even under optimized conditions, the separation achieved by column chromatography required the collection of multiple fractions and evaluated by electronic absorption and NMR spectroscopies. Attempts to grow single crystals were unsuccessful; the identity and purity of the final complexes were ultimately determined by NMR, high resolution ESI/MS, and elemental analysis.

Ground-State Spectroscopic Properties. The ground state absorption spectra of the three complexes are shown in Figure 1. Metal bipyridyl complexes typically exhibit both intraligand as well as charge-transfer transitions. On the basis of extinction coefficients as well as comparison to other ruthenium polypyridyl complexes, the UV absorption features in complexes **1**−**3** can be assigned as $\pi \rightarrow \pi^*$ absorptions of the bipyridine ligands whereas the somewhat weaker but still intense visible features are MLCT in nature; more specific assignments can be made by examining changes in the spectra across the series. For example, in complex **3** there is a single UV absorption at 315 nm which can be readily assigned as a $\pi \rightarrow \pi^*$ absorption(s) of the CN-Me-bpy ligand since that is the only type of bipyridyl ligand present. Complexes **1** and **2** also have UV absorptions at 318 and 317 nm, respectively, which are likewise assigned to $\pi \rightarrow \pi^*$ absorptions of the CN-Me-bpy ligand. The intensity of this band decreases across the series, getting progressively smaller as the CN-Me-bpy ligand is systematically replaced by bpy, further supporting this assignment. Upon introduction of the unsubstituted bpy ligand, a higher energy UV absorption appears that shows the opposite trend: this is obviously associated with the unsubstituted bipyridine ligand. The relative energies of the two absorption features are reasonable given the additional conjugation of the π system expected for the CN-Me-bpy ligand.

Assignments within the charge transfer band are not as straightforward but can be clarified using electrochemistry. To a reasonable approximation the energy of a metal-to-ligand charge transfer band can be thought of in terms of the energy required to oxidize the metal and reduce the ligand, that is, $E(MLCT) \sim E(M \rightarrow M^+) + E(L \rightarrow L^-)$ for $M\text{-}L \rightarrow M^+\text{-}L^-$.[64] For two ligands bound to the same metal, the energy of the MLCT state(s) will therefore correlate with the reduction potentials of the ligands. The electrochemical properties of complexes **1**−**3** have been investigated by cyclic voltammetry (CV) and differential pulse voltammetry (DPV), the results of which are listed in Table 1.

(50) Juris, A.; Balzani, V.; Barigelletti, F.; Campagna, S.; Belser, P.; Von Zelewsky, A. *Coord. Chem. Rev.* **1988**, *84*, 85–277.
(51) Furue, M.; Maruyama, K.; Oguni, T.; Naiki, M.; Kamachi, M. *Inorg. Chem.* **1992**, *31*, 3792–3795.
(52) Anderson, P. A.; Deacon, G. B.; Haarmann, K. H.; Keene, F. R.; Meyer, T. J.; Reitsma, D. A.; Skelton, B. W.; Strouse, G. F.; Thomas, N. C. *Inorg. Chem.* **1995**, *34*, 6145–6157.
(53) Masui, H.; Murray, R. W. *Inorg. Chem.* **1997**, *36*, 5118–5126.
(54) Pichot, F.; Beck, J. H.; Elliott, C. M. *J. Phys. Chem. A* **1999**, *103*, 6263–6267.
(55) Losse, S.; Görls, H.; Groarke, R.; Vos, J. G.; Rau, S. *Eur. J. Inorg. Chem.* **2008**, 4448–4452.
(56) Constable, E. C.; Thompson, A. M. W. C.; Harveson, P.; Macko, L.; Zehnder, M. *Chem.—Eur. J.* **1995**, *1*, 360–367.
(57) Chodorowski-Kimmes, S.; Beley, M.; Collin, J. P.; Sauvage, J. P. *Tetrahedron Lett.* **1996**, *37*, 2963–2966.
(58) Aspley, C. J.; Williams, J. A. G. *New J. Chem.* **2001**, *25*, 1136–1147.
(59) Fang, Y. Q.; Polson, M. I.; Hanan, G. S. *Inorg. Chem.* **2003**, *42*, 5–7.
(60) Kozlov, D. V.; Tyson, D. S.; Goze, C.; Ziessel, R.; Castellano, F. N. *Inorg. Chem.* **2004**, *43*, 6083–6092.
(61) Pomestchenko, I. E.; Polyansky, D. E.; Castellano, F. N. *Inorg. Chem.* **2005**, *44*, 3412–3421.
(62) Jin, F.; Confalone, P. N. *Tetrahedron Lett.* **2000**, *41*, 3271–3273.
(63) Weissman, S. A.; Zewge, D.; Chen, C. *J. Org. Chem.* **2005**, *70*, 1508–1510.

Scheme 1. Synthesis of Complexes **1**–**3**[a]

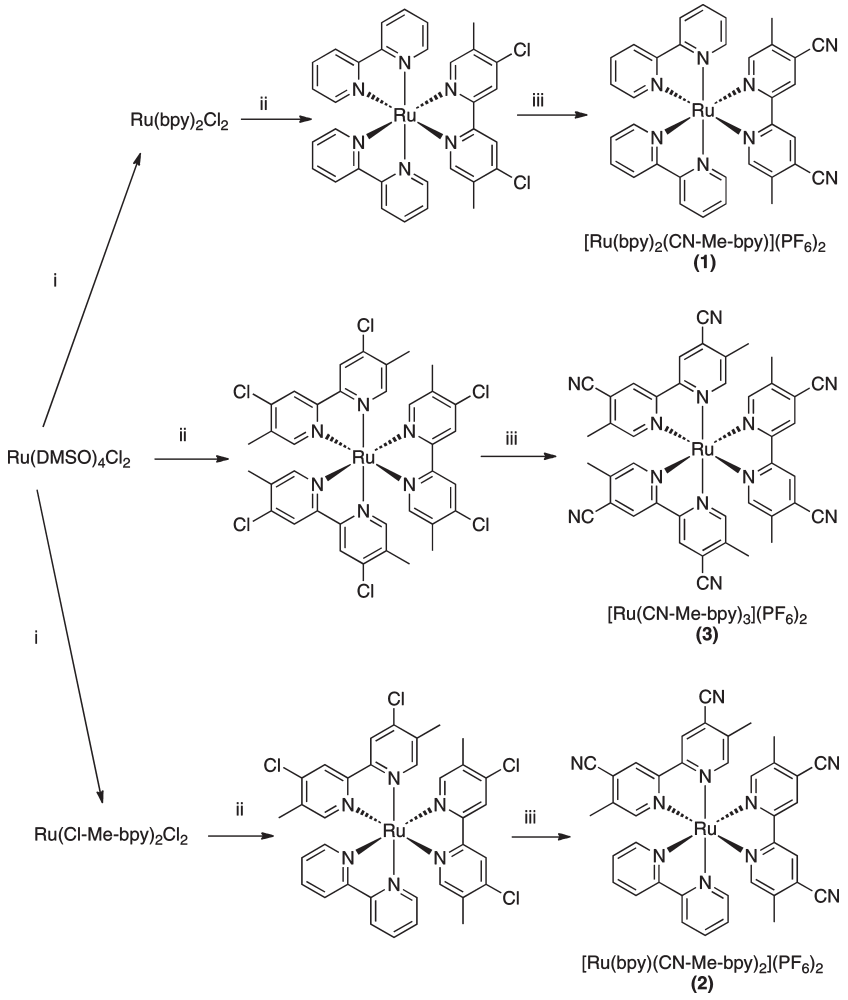

[a] (i) bpy or Cl-Me-bpy and LiCl refluxed in DMF. (ii) bpy or Cl-Me-bpy refluxed in ethanol. (iii) $Pd_2(dba)_3$, dppf, ZnCN, and zinc dust heated in DMA. See text for details.

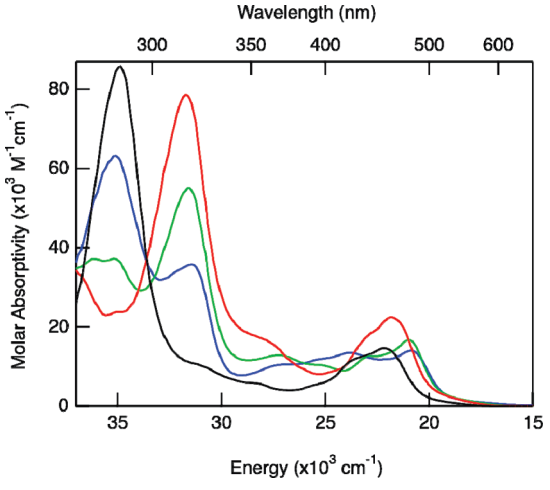

Figure 1. Electronic absorption spectra of $[Ru(bpy)_2(CN\text{-}Me\text{-}bpy)](PF_6)_2$ (**1**, blue line), $[Ru(bpy)(CN\text{-}Me\text{-}bpy)_2](PF_6)_2$ (**2**, green line), $[Ru(CN\text{-}Me\text{-}bpy)_3](PF_6)_2$ (**3**, red line), and $[Ru(bpy)_3](PF_6)_2$ (black line) in CH_3CN solutions.

The electron-withdrawing nature of the cyano group is immediately apparent from the trends in the ruthenium oxidation potential across the series. Starting with $[Ru(bpy)_3]^{2+}$, each successive replacement of 2,2′-bipyridine by CN-Me-bpy in the coordination sphere systematically shifts the oxidation potential of the metal center positive by about 130 mV. The inferred decrease in negative charge density at the ruthenium indicates the generally poorer electron donating ability of the CN-Me-bpy relative to the unsubstituted ligand. With regard to the ligand reductions, we can see by comparing the first reduction potentials of $[Ru(bpy)_3]^{2+}$ and complex **3** that the CN-Me-bpy ligand is more easily reduced than the bpy ligand by 480 mV; in both complexes, the three reduction potentials are evenly spaced with a difference of 200 ± 50 mV between each successive reduction. In complex **1**, the first reduction potential is much closer in energy to that of the first reduction of complex **3**, whereas the second and third reduction potentials are much closer to those of $[Ru(bpy)_3]^{2+}$. These observations support the notion that the first reduction potential in complex **1** is associated with the CN-Me-bpy ligand, and the second and third reductions are those of the unsubstituted bpy ligands. Analogous assignments hold for complex **2**, that is, the first and second

(64) Vlček, A. A.; Dodsworth, E. S.; Pietro, W. J.; Lever, A. B. P. *Inorg. Chem.* **1995**, *34*, 1906–1913.

Table 1. Electrochemical Data for Complexes **1**−**3** and $[Ru(bpy)_3](PF_6)_2$ in CH_3CN Solution [a]

complex	$E_{1/2}^{ox}$	$E_{1/2}^{red1}$	$E_{1/2}^{red2}$	$E_{1/2}^{red3}$	ΔE (eV)[b]	E_0 (eV)[c]
$[Ru(bpy)_3](PF_6)_2$	+0.91	−1.70	−1.89	−2.14	2.61	2.03
$[Ru(bpy)_2(CN\text{-}Me\text{-}bpy)](PF_6)_2$(**1**)	+1.01	−1.38	−1.86	−2.06	2.45	1.82
$[Ru(bpy)(CN\text{-}Me\text{-}bpy)_2](PF_6)_2$(**2**)	+1.13	−1.33	−1.52	−1.99	2.46	1.91
$[Ru(CN\text{-}Me\text{-}bpy)_3](PF_6)_2$(**3**)	+1.29	−1.25	−1.40	−1.61	2.54	1.99

[a] Potentials are reported in V versus the ferrocene/ferrocenium couple as described in the Experimental Section. [b] $\Delta E = (E_{1/2}^{ox} - E_{1/2}^{red1})$. [c] E_0 from Table 3.

reductions are the sequential reductions of the two CN-Me-bpy ligands whereas the third corresponds to reduction of 2,2′-bipyridine.

Returning to the electronic absorption spectra in Figure 1, the lower energy absorption at 479 nm can now be assigned to a $^1A_1 \rightarrow {}^1$MLCT transition associated with the CN-Me-bpy ligand, whereas the higher energy portion of the absorption band centered near 420 nm are corresponding transitions coupled to the unsubstituted bpy ligands; similar arguments apply for complex **2**. In complex **3** there is a single main visible absorption at 458 nm that obviously corresponds to MLCT transition(s) to the CN-Me-bpy ligand. It is interesting to note that the MLCT absorption in the symmetric tris complex is much narrower and appears at higher energy than its counterpart in the heteroleptic complexes **1** and **2**. This phenomenon has been seen in other series of heteroleptic ruthenium complexes. The change in breadth most likely reflects the presence of multiple absorption features because of both the reduction of symmetry (i.e., from nominally D_3 to C_2) and the overlap with transitions associated with the various ligands, whereas the difference in energy reflects the influence of the ancillary ligands on the electrochemical properties of the system.[19,51,65]

Steady-State and Time-Resolved Emission Spectroscopies. The room temperature emission spectra for all three complexes are plotted in Figure 2a. The emission maxima for $[Ru(bpy)_2(CN\text{-}Me\text{-}bpy)](PF_6)_2$ (**1**), $[Ru(bpy)(CN\text{-}Me\text{-}bpy)_2](PF_6)_2$ (**2**), and $[Ru(CN\text{-}Me\text{-}bpy)_3](PF_6)_2$ (**3**) appear at 686 nm, 658 nm, and 626 nm, respectively, following the same trend as the ruthenium oxidation potentials across the series. Radiative quantum yields were determined relative to $[Ru(bpy)_3](PF_6)_2$ and are listed in Table 2. The measured quantum yields correlate with the emission energies, increasing from 13% in complex **1** to 40% in complex **3**. While these quantum yields may seem unusually large for ruthenium polypyridyl complexes (especially that of complex **3**), many ruthenium tris bipyridine[43] and tris phenanthroline[50] complexes containing aromatic substituents exhibit radiative quantum yields on this order. In addition, the recent correction in the absolute value of Φ_r for $[Ru(bpy)_3](PF_6)_2$ from 6.2% to 9.5% must be borne in mind when comparing values in the literature.[39]

To obtain more quantitative insights into the ^{3}MLCT excited states of this system, we carried out a single mode spectral fitting analysis based on eq 2 as described by Meyer and co-workers.[41,66] The room-temperature emission spectra shown in Figure 2a are typical of molecules in this class, showing virtually no vibrational fine structure; consequently, a high degree of correlation among the four fitting

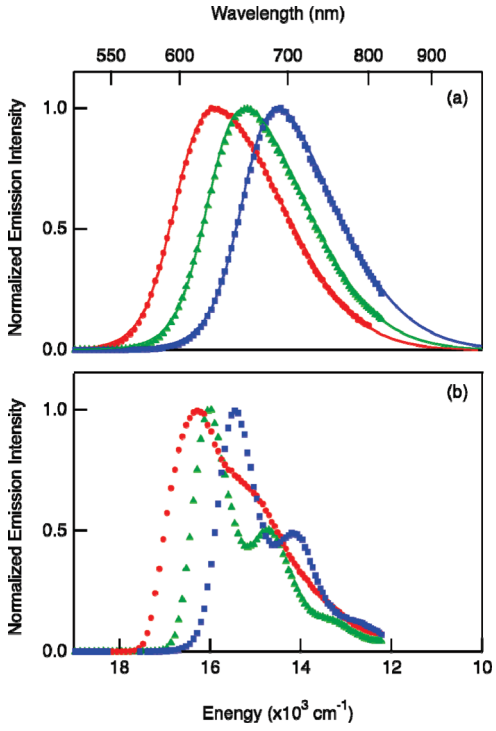

Figure 2. Steady-state emission spectra of $[Ru(bpy)_2(CN\text{-}Me\text{-}bpy)](PF_6)_2$ (**1**, blue squares), $[Ru(bpy)(CN\text{-}Me\text{-}bpy)_2](PF_6)_2$ (**2**, green triangles), and $[Ru(CN\text{-}Me\text{-}bpy)_3](PF_6)_2$ (**3**, red circles). (a) Room-temperature spectra acquired in deoxygenated CH_3CN solution. The solid lines correspond to fits to an asymmetric double sigmoidal function; see text for further details. (b) Emission spectra acquired in a 9:2 butyronitrile/propionitrile glass at 80 K.

parameters endemic to a single-mode fit (E_0, S_M, $\hbar\omega_M$, and $\Delta\bar{\nu}_{0,1/2}$) was observed, and the spectra could be fit equally well to a wide range of combined values. In a low-temperature glass, however, sufficient fine structure is resolved to help mitigate the overdetermined nature of the problem at room temperature (Figure 2b). Following the example of Claude and Meyer, the value of $\hbar\omega_M$ was assumed to be temperature independent, so the room temperature spectra were refit using the low temperature value of $\hbar\omega_M$ as a fixed parameter. Using this approach, well-defined (<10% variation) values for the ^{3}MLCT zero-point energy (E_0), Huang−Rhys factor (S_M), and the spectral bandwidth ($\Delta\bar{\nu}_{0,1/2}$) could be determined for the room-temperature spectra. Spectral fitting parameters obtained in this manner for complexes **1**−**3** and $[Ru(bpy)_3](PF_6)_2$ are listed in Table 3.

The fitted values for E_0 for all three complexes are very close to the observed emission maxima, indicating that the $\nu^* = 0 \rightarrow \nu = 0$ transition is the dominant contribution to the observed emission spectrum. The Huang−Rhys factor can be thought of as a measure of the vibrational overlap

(65) Mabrouk, P. A.; Wrighton, M. S. *Inorg. Chem.* **1986**, *25*, 526–531.
(66) Kober, E. M.; Caspar, J. V.; Lumpkin, R. S.; Meyer, T. J. *J. Phys. Chem.* **1986**, *90*, 3722–3734.

Table 2. Photophysical Data for Complexes **1**−**3** and $[Ru(bpy)_3](PF_6)_2$ in CH_3CN Solution

complex	λ_{em} (nm)	Φ_r[a]	τ_{obs} (μs)[b]	k_{obs} ($\times 10^5$ s^{-1})[b]	k_r ($\times 10^4$ s^{-1})[a,c]	k_{nr} ($\times 10^5$ s^{-1})[a,d]
$[Ru(bpy)_3](PF_6)_2$	618	0.095 ± 0.003	0.95 ± 0.01	10.5 ± 0.10	10.0 ± 0.30	9.53 ± 0.08
$[Ru(bpy)_2(CN\text{-}Me\text{-}bpy)](PF_6)_2$ (**1**)	686	0.13 ± 0.004	1.56 ± 0.02	6.41 ± 0.08	8.33 ± 0.25	5.58 ± 0.17
$[Ru(bpy)(CN\text{-}Me\text{-}bpy)_2](PF_6)_2$ (**2**)	658	0.27 ± 0.008	2.62 ± 0.04	3.82 ± 0.06	10.3 ± 0.31	2.79 ± 0.08
$[Ru(CN\text{-}Me\text{-}bpy)_3](PF_6)_2$ (**3**)	626	0.40 ± 0.012	3.50 ± 0.05	2.86 ± 0.04	11.4 ± 0.35	1.71 ± 0.05

[a] Error bars based on the 3% uncertainty in the $[Ru(bpy)_3](PF_6)_2$ quantum yield standard. [b] Uncertainty determined by the standard deviation of multiple measurements. [c] $k_r = \Phi_r \cdot k_{obs}$. [d] $k_{nr} = k_{obs} - k_r$.

Table 3. Spectral Fitting Results for Complexes **1**−**3** and $[Ru(bpy)_3](PF_6)_2$

	low temperature[a,b]				room temperature[b,c]			
complex	E_0 (cm^{-1})	S_M	$\hbar\omega_M$ (cm^{-1})	$\Delta\bar{\nu}_{0,1/2}$(cm^{-1})	E_0 (cm^{-1})	S_M	$\hbar\omega_M$ (cm^{-1})	$\Delta\bar{\nu}_{0,1/2}$(cm^{-1})
$[Ru(bpy)_3](PF_6)_2$	17220 ± 50	1.05 ± 0.06	1345 ± 40	950 ± 60	16365 ± 50	1.01 ± 0.08	1345	1740 ± 120
$[Ru(bpy)_2(CN\text{-}Me\text{-}bpy)](PF_6)_2$ (**1**)	15410 ± 40	0.67 ± 0.06	1290 ± 40	985 ± 60	14650 ± 50	0.65 ± 0.1	1290	1675 ± 110
$[Ru(bpy)(CN\text{-}Me\text{-}bpy)_2](PF_6)_2$ (**2**)	15970 ± 50	0.69 ± 0.05	1285 ± 40	950 ± 50	15410 ± 50	0.73 ± 0.09	1285	1675 ± 120
$[Ru(CN\text{-}Me\text{-}bpy)_3](PF_6)_2$ (**3**)	16335 ± 70	0.84 ± 0.07	1365 ± 90	1315 ± 90	15970 ± 70	0.79 ± 0.11	1365	1810 ± 150

[a] Fitting results for 80 K emission spectra in 9:2 butyronitrile:propionitrile. [b] Error bars represent an approximate range of visually equivalent fits. [c] Fitting results for room temperature emission spectra in CH_3CN, using a fixed value of $\hbar\omega_M$ based on the low temperature data. See text for details.

between the excited state and the ground state and is proportional to $(\Delta Q)^2$. This makes S_M a useful parameter for gauging the degree of structural distortion in the excited state relative to the ground state and in this regard is sometimes referred to as a mode-specific reduced reorganization energy (i.e., $S_M = \lambda/\hbar\omega_M$).[43] It is difficult to draw any conclusions concerning differences across the series since the variations in S_M for complexes **1**−**3** are within the uncertainties of the fits; however, all three exhibit S_M values that are smaller than that obtained for $[Ru(bpy)_3](PF_6)_2$. This result suggests that the three cyano-substituted complexes have excited-state geometries that are slightly less distorted relative to their ground states as compared to $[Ru(bpy)_3](PF_6)_2$.

The excited-state lifetimes of complexes **1**−**3** were determined using nanosecond time-resolved emission spectroscopy, from which radiative (k_r) and non-radiative (k_{nr}) decay rates were calculated (Table 2). The most significant differences across the series can be seen in the relative values of k_{nr}. As predicted by the energy gap law,[62] we note an inverse relationship between the zero-point energy differences and the rates of non-radiative decay back down to the ground state; this is not surprising and has been observed in a wide range of systems. Along the lines of the preceding discussion concerning the Huang−Rhys factor, a comparison of k_{nr} values for $[Ru(CN\text{-}Me\text{-}bpy)_3]^{2+}$ and $[Ru(bpy)_3]^{2+}$ is more instructive because of their comparable emission maxima: this effectively divides out the effect of zero-point energy and therefore reflects primarily the relative excited-state/ground-state potential energy surface displacements for the two compounds. We can see that the suggestion of a smaller value of S_M for the cyano-containing compounds from the spectral fitting analysis as compared to $[Ru(bpy)_3]^{2+}$ is confirmed by the ∼5-fold reduction in k_{nr} for compound **3**. From this result it can be concluded that the excited state in this compound (and by extension the entire series) is indeed characterized by a smaller degree of geometric distortion relative to $[Ru(bpy)_3]^{2+}$, which in turn can be reasonably ascribed to delocalization of the π^* orbital into the cyano group(s) of the CN-Me-bpy ligand.

The differences in radiative decay rate (k_r) are less dramatic than what is observed for k_{nr}, but nevertheless support the same conclusion. Radiative decay theory specifies a proportionality between k_r and the product $\mu^2 \cdot E_0^3$ (where μ is the transition dipole moment and E_0 is the energy gap[67]), and the trend in k_r for complexes **1**−**3** is wholly consistent with this picture. Turning again to a comparison of the two $[RuL_3]^{2+}$ complexes, we note that complex **3** has a radiative decay rate that is ∼10% larger than that of $[Ru(bpy)_3](PF_6)_2$ despite having a slightly smaller energy gap. This implies a larger transition dipole for complex **3**, which is again consistent with coupling of the CN group into the bipyridyl ligand insofar as this would allow delocalization of the π^* orbital into the periphery of the ligand and increase the effective magnitude of the transition dipole. A similar effect is evident in the ground-state absorption spectra (Figure 1), which clearly shows a larger oscillator strength associated with the $^1A_1 \rightarrow {}^1$MLCT absorption for complex **3** relative to $[Ru(bpy)_3](PF_6)_2$. Previous work from our lab on a series of aryl-substituted ruthenium(II) polypyridyl complexes revealed similar trends in k_r and k_{nr} that were attributed to an extended π system in the MLCT manifold.[43]

Time-Resolved Electronic Absorption Spectroscopy. Nanosecond transient absorption spectroscopy is another important tool for characterizing the lowest energy excited states of transition metal complexes, particularly as a precursor to ultrafast spectroscopic measurements.[29] Transient absorption spectra of complexes **1**−**3** and $[Ru(bpy)_3](PF_6)_2$ acquired following $^1A_1 \rightarrow {}^1$MLCT excitation are shown in Figure 3. There are three principle features observed in all of the spectra: a strong net absorption in the near-UV, a strong bleach in the midvisible, and a weak absorption extending into the red. This overall pattern is typical of what is observed for the excited-state spectra of Ru^{II} polypyridyl complexes.

Since an MLCT excited state can be thought of in terms of an oxidized metal and a reduced ligand (vide supra), spectroelectrochemistry can be a useful guide for making

(67) Kestner, N. R.; Logan, J.; Jortner, J. *J. Phys. Chem.* **1974**, *78*, 2148–2166.

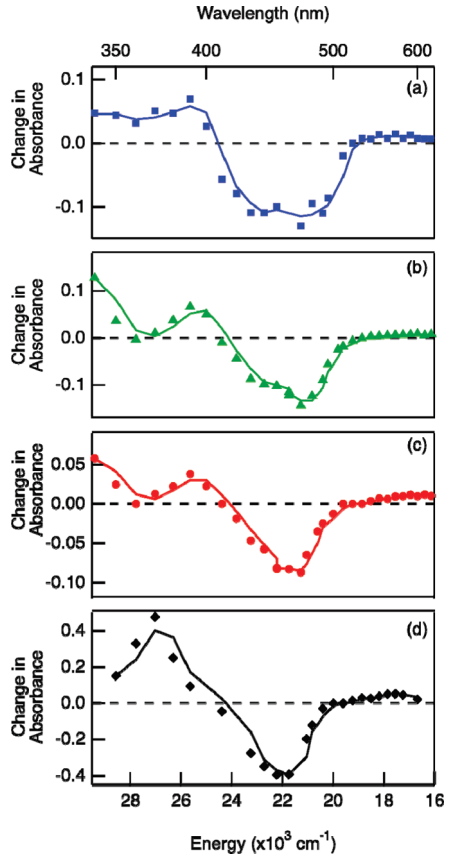

Figure 3. Nanosecond time-resolved differential absorption spectra acquired in room-temperature CH_3CN solution for (a) $[Ru(bpy)_2(CN\text{-}Me\text{-}bpy)](PF_6)_2$ (**1**), (b) $[Ru(bpy)(CN\text{-}Me\text{-}bpy)_2](PF_6)_2$ (**2**), (c) $[Ru(CN\text{-}Me\text{-}bpy)_3](PF_6)_2$ (**3**), and (d) $[Ru(bpy)_3](PF_6)_2$. The individual points correspond to the amplitudes of fits of the kinetics data to single-exponential decay models; a smoothed solid line has been included in each plot to guide the eye.

assignments as to the specific origins of the various features. The change in absorbance upon oxidation of complex **1** is shown in Figure 4b. When the Ru^{II} center is oxidized to Ru^{III}, the dominant feature in the differential spectrum is the loss of the MLCT absorption band in the visible. In addition, we note that the $\pi \rightarrow \pi^*$ absorption of the CN-Me-bpy ligand, which occurs at ~315 nm in the ground state spectrum (Figure 1), shifts to ~340 nm when coordinated to Ru^{III}. The weak absorption at 725 nm shown in the inset can be assigned as an LMCT absorption based on comparison to other reported Ru^{III} polypyridyl complexes.[68] Upon reduction of the parent compound (Figure 4c), strong absorptions associated with the radical anion of the ligand are seen across the UV and visible portions of the spectrum. A small bleach is also seen in the midvisible because of the loss of the charge-transfer transition to the CN-Me-bpy ligand that has undergone reduction. Spectroelectrochemical data for complexes **2** and **3** can be found in the Supporting Information, Figures S4 and S5. While there are qualitative differences in the spectral profiles (due primarily to differences in the ground state absorption spectra), analogous conclusions hold for these compounds.

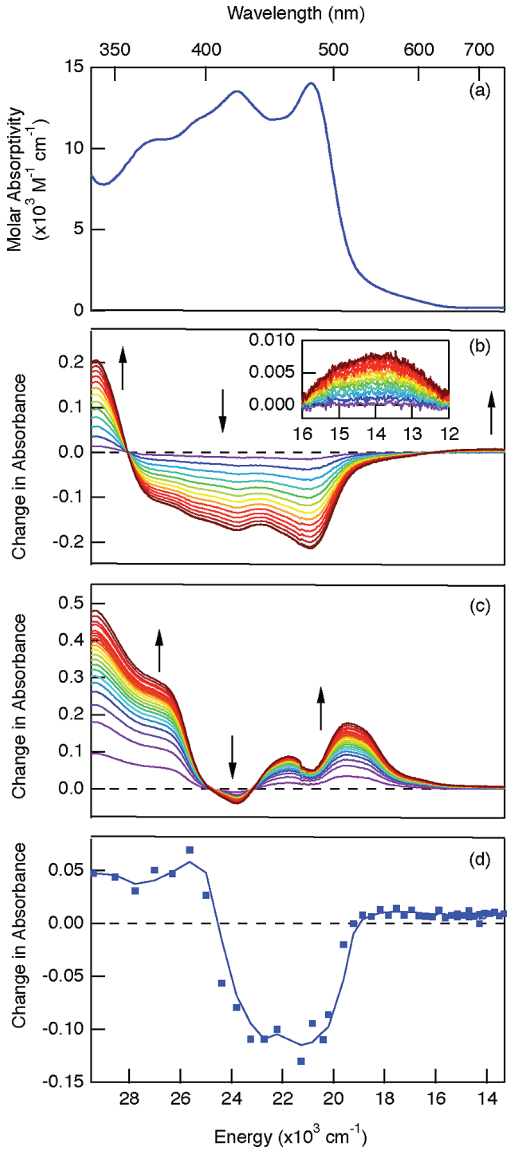

Figure 4. (a) Ground state absorption spectrum for $[Ru(bpy)_2(CN\text{-}Me\text{-}bpy)](PF_6)_2$ (**1**) in room-temperature CH_3CN solution. (b) Oxidative difference spectra acquired at an applied potential of +1.55 V versus Ag/AgCl. The inset corresponds to an expanded view of the low-energy portion of the spectrum. (c) Reductive difference spectra acquired at an applied potential of −1.05 V versus Ag/AgCl. (d) Time-resolved differential absorption spectrum of compound **1** following excitation at 500 nm.

It is difficult to make a quantitative comparison of the combined spectroelectrochemical data and the differential absorption spectrum of the corresponding charge-transfer state because not all contributions to the latter can be accurately accounted for;[69] however, reasonable assignments can still be made. The strong net bleach in the midvisible is obviously due to the loss of the ground-state $^1A_1 \rightarrow {}^1$MLCT absorption upon formation of the excited state. Other regions are potentially more complicated because the transient absorption spectrum of the ^{3}MLCT state reflects a superposition of the complete loss of ground-state absorption and new absorptions associated with the ^{3}MLCT chromophore; the differential nature of the measurement also means that small shifts in absorption maxima

(68) Nazeeruddin, M. K.; Zakeeruddin, S. M.; Kalyanasundaram, K. *J. Phys. Chem.* **1993**, *97*, 9607–9612.

(69) Brown, A.; Smeigh, A. L.; McCusker, J. K., manuscript in preparation.

(e.g., a ligand radical bound to Ru^{III} as opposed to Ru^{II}) can result in significant modulation of the observed spectrum. These points notwithstanding, the most striking aspect of Figure 3 is the similarity among the three CN-Me-bpy-containing complexes as compared to $[Ru(bpy)_3](PF_6)_2$, especially in the near-UV region, suggesting a common character to the excited states being sampled. Furthermore, the significant red shift of the near UV feature in complexes **1**−**3** relative to $[Ru(bpy)_3](PF_6)_2$ suggests that the ^{3}MLCT excited states of complexes **1**−**3** are of a distinctly different character from that found in $[Ru(bpy)_3](PF_6)_2$. Given that the electrochemical data indicated that the CN-Me-bpy ligand was the most easily reduced in complexes **1**−**3** (and should therefore house the ^{3}MLCT excited state being sampled in these measurements), we can immediately conclude from these results that the positive differential absorption near 380 nm in complexes **1**−**3** is due to the CN-Me-bpy radical anion. The lowest-energy ^{3}MLCT state in all three members of this series can therefore be approximately described as Ru^{III}-(CN-Me-bpy^-) in nature.

Finally, wavelengths to the red of the ground state/excited state isosbestic point at 520 nm have contributions from both the CN-Me-bpy radical anion as well as LMCT transition(s) involving the ancillary bpy ligands. There is a canceling effect operative in this region of the differential spectrum because of the relatively weak intensity of these absorptive features and the tail of the ground-state charge-transfer band. The net result is a generally featureless, weak transient signal of the kind evident in Figure 3 that is typical for Ru^{II} polypyridyl complexes.

Nanosecond Step-Scan Time-Resolved Infrared Spectroscopy. As mentioned in the introduction, our primary goal in developing this series of compounds was to use them as probes for vibrational relaxation dynamics in charge-transfer excited states. Similar to our protocol for studying the ultrafast electronic absorption spectroscopy of transition metal chromophores,[29] it is important to fully characterize the vibrational properties of the long-lived excited state as a foundation for interpreting data acquired on shorter time scales.

Both time-resolved resonance Raman (TR^3) and time-resolved infrared (TRIR) methods have been developed; each technique has advantages and disadvantages. In TR^3 visible light is used to create as well as resonantly scatter off the excited state. The resonance condition means that only those vibrations that are coupled to the excited electronic transition are enhanced. This can vastly simplify the spectrum and assigning the nature of the excited state, but at the same time gives only a partial picture of the excited state vibrational structure. From a technical perspective, interference from emission can also make using this technique on highly emissive compounds challenging. With TRIR the entire vibrational spectrum of the excited state is sampled using an infrared probe beam, thereby providing a more complete picture of the excited state vibrational structure but can make interpretation more difficult. TRIR has been used to characterize

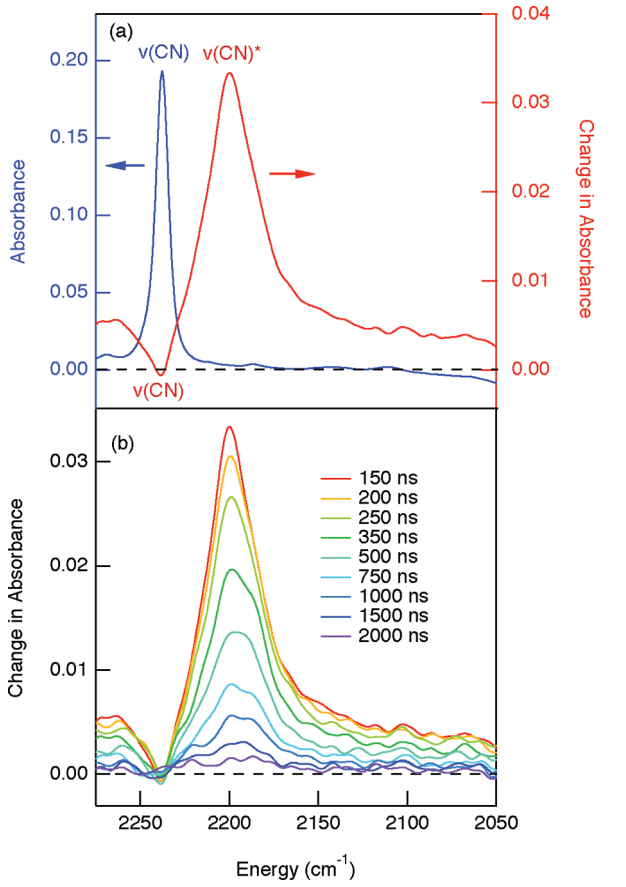

Figure 5. Steady-state and time-resolved infrared absorption data for $[Ru(bpy)_2(CN\text{-}Me\text{-}bpy)](PF_6)_2$ (**1**) in room-temperature CH_3NO_2 solution. (a) Comparison of the ground state (blue line) and step-scan infrared differential absorption data acquired at a time delay of 150 ns following excitation at 540 nm (red line). The ~40 cm^{-1} red-shift in the CN stretching frequency reflects the presence of an electron in the π^* orbital of the CN-Me-bpy ligand in the ^{3}MLCT excited state. (b) Nanosecond step-scan infrared spectra as a function of time following excitation at 540 nm. The kinetics describing the decrease in amplitude of the excited state infrared absorption signal are within experimental error of the time-resolved emission and absorption data for compound **1** and are therefore assigned to relaxation of the ^{3}MLCT excited state. The baseline offset in the excited state infrared absorption spectra is an artifact caused by a signal-induced bias of the detector.

the vibrational structure of long-lived excited states for a variety of systems.[70−72] Previous work from our group employed TRIR on a series of heteroleptic ruthenium polypyridyl complexes to identify on which ligand the emissive excited state was localized.[19] Relevant to the present study, Meyer, Palmer, and co-workers examined a series of ruthenium polypyridyl complexes substituted with diethyl ester and diethyl amide groups as infrared tags.[73,74] These workers were able to demonstrate localization of the long-lived excited state on a single bipyridine ligand for both heteroleptic and homoleptic complexes, including an interesting example of a 4-monosubstituted

(70) Omberg, K. M.; Schoonover, J. R.; Treadway, J. A.; Leasure, R. M.; Dyer, R. B.; Meyer, T. J. *J. Am. Chem. Soc.* **1997**, *119*, 7013–7018.
(71) Omberg, K. M.; Schoonover, J. R.; Bernhard, S.; Moss, J. A.; Treadway, J. A.; Kober, E. M.; Dyer, R. B.; Meyer, T. J. *Inorg. Chem.* **1998**, *37*, 3505–3508.
(72) Yeom, Y.; Frei, H. *In-situ Spectroscopy of Catalysts*; American Scientific Publishers: Valencia, CA, 2004; pp 32−46.
(73) Chen, P.; Omberg, K. M.; Kavaliunas, D. A.; Treadway, J. A.; Palmer, R. A.; Meyer, T. J. *Inorg. Chem.* **1997**, *36*, 954–955.
(74) Omberg, K. M.; Smith, G. D.; Kavaliunas, D. A.; Chen, P.; Treadway, J. A.; Schoonover, J. R.; Palmer, R. A.; Meyer, T. J. *Inorg. Chem.* **1999**, *38*, 951–956.

Table 4. Step-Scan IR and DFT Results for Complexes **1**−**3**

Nanosecond Time-resolved Scan IR			
	$\bar{\nu}(CN)_{GS}$ (cm^{-1})[a]	$\bar{\nu}(CN)_{MLCT^3}$ (cm^{-1})[b]	$\Delta\bar{\nu}$ (CN) (cm^{-1})[c]
$[Ru(bpy)_2(CN\text{-}Me\text{-}bpy)](PF_6)_2$ (**1**)	2238	2200	−38
$[Ru(bpy)(CN\text{-}Me\text{-}bpy)_2](PF_6)_2$ (**2**)	2238	2200	−38
$[Ru(CN\text{-}Me\text{-}bpy)_3](PF_6)_2$ (**3**)	2239	2202	−37
DFT Frequency Calculations			
	$\bar{\nu}(CN)_{GS}$ (cm^{-1})[d,e]	$\bar{\nu}(CN)_{MLCT^3}$ (cm^{-1})[e,f]	$\Delta\bar{\nu}$ (CN) (cm^{-1})[c]
$[Ru(bpy)_2(CN\text{-}Me\text{-}bpy)](PF_6)_2$ (**1**)	2272 (as)	2216 (as)	−56 (as)
	2272 (s)	2237 (s)	−35 (s)

[a] Ground state absorption maximum in CH_3NO_2 solution (4 cm^{-1} resolution). [b] Excited state differential absorption maximum in CH_3NO_2 solution (4 cm^{-1} resolution). [c] $\Delta\bar{\nu}$ (CN) = $\bar{\nu}(CN)_{MLCT^3} - \bar{\nu}(CN)_{GS}$. [d] Frequency calculation results on the ground state optimized geometry. [e] (s) is the totally symmetric CN stretching frequency, (as) is the asymmetric CN stretching frequency. [f] Frequency calculation results on the lowest energy triplet state optimized geometry.

bipyridine ligand in which the long-lived excited state was primarily localized on the substituted pyridine ring containing the electron-withdrawing group rather than being symmetrically distributed across the entire ligand. Collectively, these studies clearly demonstrate the utility of nanosecond step-scan infrared for characterizing this class of compounds.

Nanosecond step-scan IR spectra of complex **1** are shown in Figure 5. The ground state exhibits a single CN band at 2238 cm^{-1}. A group theoretical analysis indicates that both the a_1 (symmetric) and b_2 (asymmetric) CN vibrations of the CN-Me-bpy ligand should be IR-active; a ground state DFT frequency calculation on complex **1** (Table 4) indeed predicts two bands, but they are calculated to be separated by < 1 cm^{-1}. The single, fairly sharp feature in Figure 5a therefore presumably contains both of these vibrations, their accidental degeneracy an indication of (relatively) weak coupling of the two CN groups in the ground state. The step-scan IR data reveals two significant features of the vibrational properties of the ^{3}MLCT excited state of compound **1**: (1) the CN stretching frequency is shifted about 40 cm^{-1} lower in energy relative to the ground state, and (2) the vibrational band is significantly broadened as compared to the sharp feature observed for the ground state. The bathochromic shift is consistent with the population of a π^* antibonding orbital, which if coupled to the cyano group should reduce the CN bond order. The magnitude of the shift is comparable to those seen by Meyer and co-workers for the amide- and ester-substituted compounds and is in-line with our expectations based on the model we have developed thus far.[73,74]

The increased breadth of the absorption feature was unexpected and suggests that the coupling between the two cyano groups has increased in the excited state such that the splitting between the a_1 and b_2 vibrations, though not fully resolved, is experimentally manifested. To gain further insight, we carried out a DFT frequency calculation on the geometry-optimized ^{3}MLCT excited state of compound **1**. These calculations indicate that $\Delta\bar{\nu}$, that is, the a_1/b_2 splitting, has increased to ~20 cm^{-1} in the excited state. The underlying reason for this change can be inferred by examining the wave functions corresponding to the ground and excited states of compound **1**. In Figure 6 are plotted the highest energy π-bonding and lowest energy π^*-antibonding orbital localized on the CN-Me-bpy ligand. In the ground state (Figure 6a), it can be seen that the π bonding orbitals of the cyanide groups have minimal interaction with the π bonding orbital of the bipyridine ring. Although this directly relates to electronic and not vibrational coupling, it is reasonable to extrapolate this as the main reason for the negligible splitting between the symmetric and asymmetric CN vibrations in the ground state. The situation is dramatically different in the ^{3}MLCT excited state (Figure 6b), in which there is substantial mixing between the π^*-antibonding orbitals of the cyanide and bipyridyl groups. This is of course why we observe the bathochromic shift in the CN stretching frequency, but it is also the likely origin of the increased spectral bandwidth of the SSIR signal as the π^* system of the bipyridyl ligand provides a conduit for communication between the peripheral groups across the ring system. We believe these results bode well for the use of these compounds as probes of ultrafast dynamics, particularly with regard to comparative studies of electronic and vibrational processes, because of the strong coupling of the infrared tag into the electronic wave function(s) involved in charge-transfer excitation.

Nanosecond step-scan IR data for complexes **2** and **3** are summarized in Table 4; the spectra can be found in the Supporting Information, Figures S6 and S7. Within experimental error the ground-state and excited-state absorption maxima are at the same energy in all three complexes. This is compelling evidence that the long-lived excited state is localized on a single CN-Me-bpy ligand in all three complexes rather than being delocalized over multiple ligands in complexes **2** and **3**. This is in agreement with previous step-scan IR studies[73,74] and is consistent with the widely held view that the ^{3}MLCT excited states of ruthenium polypyridyl compounds in solution are best thought of as localized (C_2-symmetry) systems.

Concluding Comments

We have described the synthesis and spectroscopic characterization of a series of cyano-substituted ruthenium polypyridyl complexes of the form $[Ru(bpy)_{3-n}(CN\text{-}Me\text{-}bpy)_n](PF_6)_2$. While these complexes could not be synthesized in

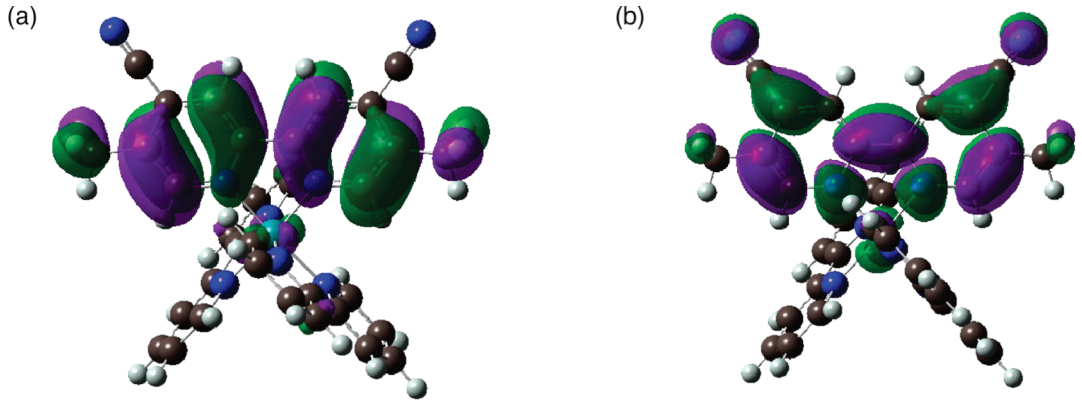

Figure 6. (a) Highest energy π bonding orbital of CN-Me-bpy in the geometry optimized ground state of complex **1**. (b) Lowest energy π^* antibonding orbital of CN-Me-bpy in the geometry optimized lowest energy triplet state of complex **1**.

reasonable amounts by combining the ligand and ruthenium starting material under standard conditions, the chemistry-on-the-complex approach proved useful. By first synthesizing the chloro-substituted ruthenium complexes and using a palladium-catalyzed cyanation reaction, it was possible to prepare and isolate all three CN-containing members of the $[Ru(bpy)_{3-n}(CN\text{-}Me\text{-}bpy)_n](PF_6)_2$ series with reasonable yield having a high degree of purity.

The ground- and ^{3}MLCT-state properties of this series have been characterized using electrochemical, optical, and infrared spectroscopies. As expected, the CN stretch of the CN-Me-bpy ligand sits in a well-isolated region of the infrared, allowing for an unambiguous analysis of its spectroscopic signatures in the ground and excited state(s) of these compounds. The data we have presented definitively show that the lowest energy charge-transfer states in all three compounds are localized on the CN-containing ligand. In particular, time-resolved electronic and infrared absorption spectroscopies reveal an identical optical signature for the ^{3}MLCT state for each compound in the series; in the case of the infrared measurements, the common shift in the CN stretching frequency indicates that (a) the CN group is strongly coupled to the π^* system of the bipyridyl ligand, and (b) that the ^{3}MLCT state is localized on a single ligand on the vibrational time scale, even in the case of the tris-homoleptic complex $[Ru(CN\text{-}Me\text{-}bpy)_3]^{2+}$. The unexpected increase in spectral bandwidth of the CN vibration(s) further revealed that the two CN groups of the ligand are more strongly coupled to each other in the ^{3}MLCT state relative to the ground state.

All of the features just enumerated underscore the potential utility of these compounds as probes of vibrational dynamics in charge-transfer excited states. With the ground and excited state spectroscopic features of this series now fully characterized, an examination of vibrational relaxation as well as the more elusive process of intramolecular vibrational redistribution is now accessible through the combined application of femtosecond time-resolved electronic and infrared absorption spectroscopies. Studies along these lines are currently underway.

Acknowledgment. The authors would like to thank Dr. Heinz Frei of the Physical Biosciences Division of the Lawrence Berkeley National Laboratory for assistance in setting up the SSIR experiment and Andrew Kouzelos for assistance with low temperature emission measurements and calculations. This research was supported by the U.S. Department of Energy, Office of Basic Energy Sciences, Chemical Sciences, Geosciences, and Biosciences Division under Grant DE-FG02-01ER15282.

Supporting Information Available: Figures of reaction progress monitoring for compounds **1**−**3** and spectroelectrochemistry and SSIR for complexes **2** and **3**. This material is available free of charge via the Internet at http://pubs.acs.org.